PHILOSOPHICAL TRANSACTIONS OF THE ROYAL SOCIETY A MATHEMATICAL, PHYSICAL & ENGINEERING SCIENCES

Collisions between Liquid Drops

S. G. Bradley and C. D. Stow

Phil. Trans. R. Soc. Lond. A 1978 **287**, 635-675
doi: 10.1098/rsta.1978.0001

COLLISIONS BETWEEN LIQUID DROPS

By S. G. BRADLEY‡ and C. D. STOW†
† *Department of Physics, The University of Auckland, Auckland, New Zealand*
‡ *New Zealand Meteorological Service, Wellington, New Zealand*§

(*Communicated by E. G. Bowen, F.R.S. – Received* 22 *June* 1976, *revised* 14 *April* 1977)

[Plates 1–3]

CONTENTS

§ Present address: Division of Cloud Physics, CSIRO, Epping, N.S.W. Australia.

Vol. 287. A 1349. 66 [Published 18 January 1978

I. THE BEHAVIOUR OF LARGE WATER DROPS COLLIDING DURING FREE FALL

An experiment is described in which pairs of water drops of different size were caused to collide during free fall at a velocity equal to the difference of their terminal velocities in still air. The collision parameters of trajectory, drop size, and drop charge were controlled with precision, and impacts of a particular kind could be reproduced indefinitely. By using synchronized flash photography, well in excess of 30 000 measurements were taken from more than 10 000 frames of film of the resulting behaviour of the water-drop pairs.

Data are discussed in terms of an impact parameter, X, which defines the relative trajectory of the drops in the centre-of-mass frame, and three energy parameters e_{C}, e_{R} and e_{T} which delineate the properties electrostatic energy, rotational energy, and total energy of the two-drop system before impact. Input parameters were confined to values appropriate to natural rainfall.

After collision four basic types of rotation occurred, the particular kind of rotation depending upon X, e_{C}, e_{R} and e_{T}. Measured rates of rotation were compared with that to be expected from a simple model of inelastic collision between solid spheres and showed a marked resemblance. Distributions of mass after collision were compared with a model based upon a bimodal Gaussian distribution to good effect. In addition, frequency distributions of the number of drop products resulting from a given collision were prepared showing the controlling influence of the impact parameter, X, and the effect of varying drop charge. Relations were also established between statistical values for the coalescence efficiency of a given drop pair and the input parameters; however, while all results were consistent and reproducible, the effect of drop charge could not be demonstrated by a simple model.

INTRODUCTION

Numerous experiments have been performed to determine numerical values for the collision efficiency of pairs of drops of different size which impact during free fall. Data have been analysed to determine the criteria for coalescence, subsequent disruption, and also to examine

the general dynamical behaviour of the two-drop system. Schotland (1960) investigated collisions between electrically neutral drops of radius 100–400 μm and a hemispherical target and determined that the onset of coalescence was dependent on the Weber number, We [$We = \rho V_N^2 D/\sigma$, where ρ is the drop density, D the drop diameter, V_N the normal velocity component, and σ the surface free energy. Coalescence occurred for $We > 3$, whereas bounce occurred at low speeds. This dimensionless number is a measure of the ratio of the inertial force to the surface force and has been shown by Schotland (1960), Foote (1975) and Sartor & Abbott (1972) to be of fundamental importance. Magarvey & Geldart (1962) appear to have been the first to study drops of a wide radius range colliding at their relative terminal velocities. Unfortunately their control of the collision was poor and their resulting data were largely qualitative, but some statistics on wake capture, temporary fusion, and coalescence were compiled.

The first useful quantitative study of the drop collision problem was that of Adam, Lindblad & Hendricks (1968). They made a careful investigation of the effect of varying the impact parameter, X, where X is defined as the ratio of the distance between droplet trajectories in their centre-of-mass frame to the sum of the drop radii. More recent investigations of the collision process have been performed by Montgomery (1971), Brazier-Smith, Jennings & Latham (1971), Spengler & Gokhale (1973) and McTaggart-Cowan & List (1975). The work of Montgomery, and of Spengler & Gokhale, produced little quantitative data, and the work of Brazier-Smith *et al.* suffered from confinement of their analysis largely to collisions between drops of equal size with no attempt to study impacts at relative terminal velocities. McTaggart-Cowan & List made considerable efforts to reproduce the conditions obtaining during natural rainfall and devised a means of accelerating their large drops to their terminal velocities. They investigated the collision and breakup of pairs of drops of different size, but while their data gave useful information on the statistical nature of collision products, their control of the collision parameters was very poor and consequently no quantitative data on the influence of the impact parameter X were possible. In the context of the work described here, the work of Adam *et al.* (1968) thus emerges as the most useful previous investigation of the problem of drop collision under natural free-fall conditions.

In the experiments described below, the collision and subsequent behaviour of water drops of unequal size has been investigated. Though falling at somewhat less than their terminal velocity, the water drops were caused to collide at a relative velocity equal to the difference of their terminal velocities and with precise control of the impact parameter, X. In these experiments aerodynamic forces are about two orders of magnitude smaller than the forces of collision and consequently, although drops were not fully deformed by the airflow, the results are thought to be applicable to calculations on the genesis of natural raindrop size distributions. The influence of drop charge on the collisions was investigated independently of other input parameters.

Selection of the input parameters

Since there is a lack of definitive data on collisions between drops falling freely in air, there follows an examination of the problem to determine what sizes of water drops might best be studied in a limited investigation and also a derivation of a set of energy parameters which describe the conditions of collision. The treatment follows similar lines to that of Cohen, Plasil & Swiatecki (1974), though these workers were, in fact, considering possible configurations of idealized atomic nuclei.

PHILOSOPHICAL TRANSACTIONS OF THE ROYAL SOCIETY A MATHEMATICAL, PHYSICAL & ENGINEERING SCIENCES

First, consider the condition in which the two colliding drops coalesce into a single liquid mass. The motion of the resulting drop is described by an energy equation,

$$E_K + E_D = E_T, \tag{I 1}$$

where E_K is the kinetic energy not associated with rotation of the drop, E_D corresponds to the energy which is associated with deformation, and E_T is the total available energy (which is constant for a particular collision). The quantity E_D may be expressed in terms of three further quantities,

$$E_D = E_S + E_C + E_R, \tag{I 2}$$

where E_S is the surface free energy, E_C the electrostatic energy and E_R the rotational energy of the drop.

Each of the energy terms in equations (I 1) and (I 2) may be divided into two parts, one a function of drop shape only, and the other a scale factor denoting the contribution of the energy term in a particular collision. If the combined liquid mass in its undeformed state forms a sphere of radius R_0, then we may denote by E_S^0, E_C^0, E_R^0, E_D^0 and E_T^0 the appropriate energy contributions. The energy of deformation and the kinetic energy may now be written in the dimensionless forms

$$\begin{aligned}\xi_D &= (E_D - E_D^0)/E_S^0 = (E_S - E_S^0 + E_C - E_C^0 + E_R - E_R^0)/E_S^0 \\ &= (A_S - 1) + 2e_C(A_C - 1) + e_R(A_R - 1)\end{aligned}$$

and

$$\begin{aligned}\xi_K &= E_K/E_S^0 = (E_T - E_D)/E_S^0 \\ &= e_T - A_S - 2e_C A_C - e_R A_R,\end{aligned} \tag{I 3}$$

where A_S, A_C and A_R are the surface, electrostatic and rotational energies of the drop, normalized with respect to the corresponding quantities for the sphere of radius R_0; they are functions of shape only, thus

$$A_S \text{ (shape)} = E_S/E_S^0, \tag{I 4a}$$

$$A_C \text{ (shape)} = E_C/E_C^0, \tag{I 4b}$$

$$A_R \text{ (shape)} = E_R/E_R^0. \tag{I 4c}$$

The dimensionless quantities, e_C, e_R and e_T are independent of drop shape and are normalized parameters which are the ratios of the electrostatic, rotational, and total energies of the sphere of radius R_0 to its surface energy (charge, angular momentum, and total energy are conserved). Thus

$$e_C = E_C^0/2E_S^0, \quad e_R = E_R^0/E_S^0, \quad e_T = E_T^0/E_S^0.$$

The parameter e_R is a measure of the size of the disruptive centrifugal forces compared to the cohesive surface tension forces. Similarly, e_C is a measure of the disruptive electrostatic forces. The factor 2 occurs in the definition of e_C so that $e_C = 1$ corresponds to the condition of a sphere of radius R_0 bearing the maximum charge determined by Rayleigh (1882). The energy terms for the sphere are

$$E_S^0 = 4\pi R_0^2 \sigma,$$

$$E_C^0 = \frac{1}{4\pi\epsilon_0}\frac{1}{2}\frac{Q_0^2}{R_0} + 4\pi\epsilon_0 \tfrac{1}{2}E_0^2 R_0^3,$$

$$E_R^0 = \frac{1}{2}\frac{5\Omega^2}{2M_0 R_0},$$

where E_0 is the undisturbed electric field in the absence of the drop, Q_0 is the total charge on the drop, M_0 the mass of the drop, and Ω its angular momentum.

Specification of the numbers e_C, e_R and e_T, which are readily determined in the laboratory, will delineate the energy characteristics of any given collision; the dynamical functions A_S, A_C and A_R do not require discussion in the context of input parameters. If the drop pair possess radii R and r, and U is the speed of approach along their trajectories, and if X is the impact parameter measured in the centre-of-mass frame, then

$$e_C = -\left[\frac{1}{4\pi\epsilon_0}\frac{Q_0^2}{16\pi R_0^3\sigma} + 4\pi\epsilon_0\frac{E_0^2 R_0}{16\pi\sigma}\right], \tag{I 5a}$$

$$e_R = \frac{5\rho R^6 r^6 (R+r)^6 U^2 X^2}{12\sigma R_0^{13}}, \tag{I 5b}$$

$$e_T = \frac{\rho R^3 r^3 U^2}{6\sigma R_0^5} + \frac{R^2+r^2}{R_0^2}, \tag{I 5c}$$

where

$$R_0 = (R^3+r^3)^{\frac{1}{3}}.$$

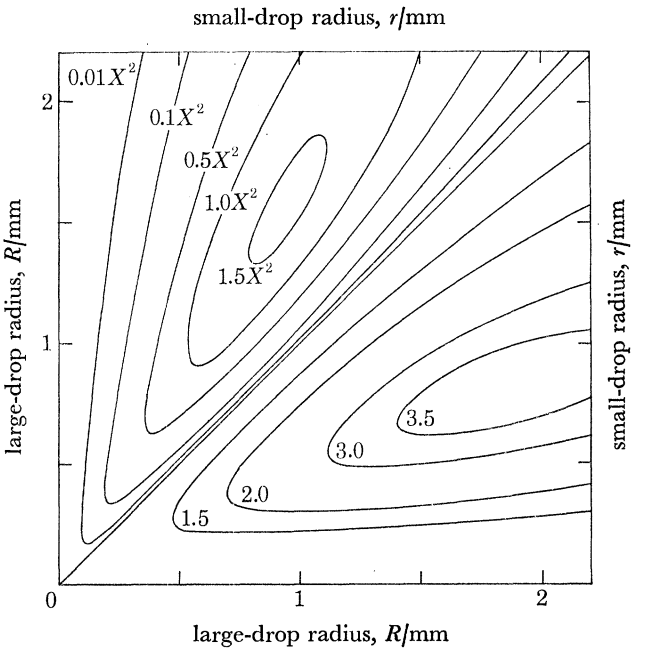

FIGURE 1. The variation with drop radii of the rotational energy parameter, e_R (above the diagonal) and total energy parameter, e_T (below the diagonal). The contours of rotational energy are expressed in terms of the impact parameter, X.

For water drops falling at their terminal velocity in air, contours of the quantities e_R and e_T (the former measured in terms of the impact parameter X) may be plotted as a function of the independent variables R and r; these contours are displayed in figure 1. The range of these parameters is

$$0 \leqslant e_R \leqslant 1.57\,X^2, \quad 1 \leqslant e_T \leqslant 3.6.$$

The lower limit of e_T occurs when $R \gg r$, and upper limits for both e_R and e_T are determined by the natural limits of drop size before aerodynamical breakup. The parameter e_R peaks at $R = 1.7$ mm and $r = 1.0$ mm, whereas the parameter e_T peaks at $R = 1.9$ mm and $r = 0.8$ mm. It is evident that the number of collisions with parameters in the range e_R to $e_R + de_R$, and e_T to $e_T + de_T$ is a maximum where (e_r, e_T) is stationary with respect to (R, r), whence from figure 1

it may be seen that collisions are most frequent in the vicinity $R = 1.5\,\text{mm}$ and $r = 1\,\text{mm}$. Clearly this region of interest should receive particular attention. Interactions involving drops of radius less than 0.5 mm will involve little rotational or total energy and can be expected to produce only stable coalescence or bounce, and are therefore of minor interest here.

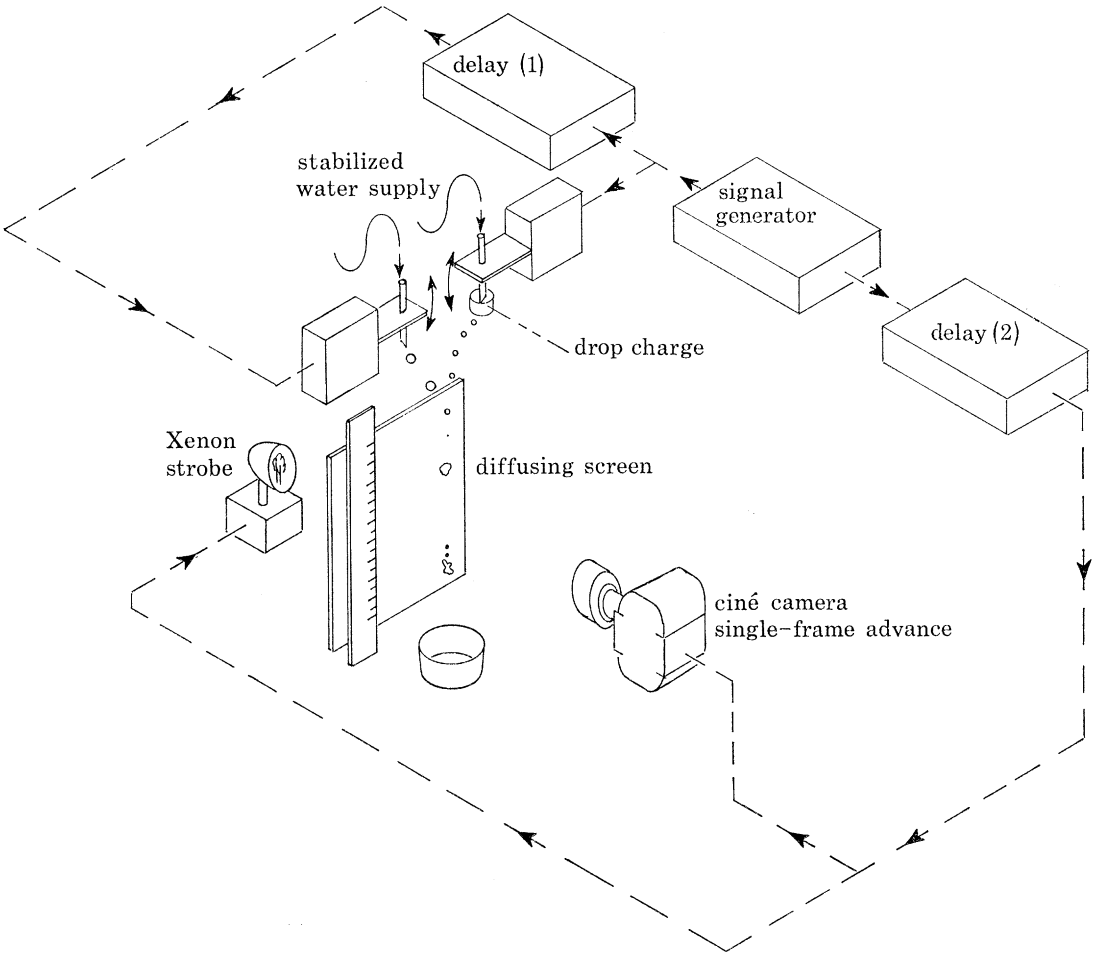

FIGURE 2. A schematic of the experimental arrangement used to obtain the drop-collision photographs.

The electrostatic component is ignored in discussions of drop trajectory, since the value of the parameter e_C is usually of the order 10^{-7}, but the equations of motion do not by themselves predict drop stability after impact. Solution of the equations of motion follows from the insertion of initial conditions, which provide values for A_S, A_C, and A_R, at the beginning of the interaction. These initial conditions describe drop shape and rate of change of shape, and would be expected to depend on the time at which the air film is ruptured. This is because no surface tension forces exist between the impacting drops until the air film between them is ruptured and a liquid bridge created. If this cohesive force is applied when the net motion is inward, coalescence is likely to occur with less probability of subsequent disruption than if the net motion were otherwise. Thus the delay in film drainage is intimately linked to drop stability and, since electrical charges may be present, the influence of the parameter e_C cannot be ignored in discussions of drop behaviour after impact. The problem of film drainage is discussed in part II of this paper.

PHILOSOPHICAL TRANSACTIONS OF THE ROYAL SOCIETY A MATHEMATICAL, PHYSICAL & ENGINEERING SCIENCES

The drop collision experiment

A schematic of the experimental arrangement is given in figure 1.2. Two streams of drops of uniform size were produced using vibrating hollow-needle generators similar to that of Gunn (1965*a*). Four sizes of needle, labelled A, B, C and D, were used giving six combinations of drop size, namely AB, AC, AD, BC, BD and CD. Careful adjustment of the relative positions of the drop generators and their relative phase of vibration (the latter using delay (1)) enabled repetitive collisions to be set up for any value of the impact parameter X with the relative velocity at impact equal to the difference in terminal velocities of the pair of drops generated. The time interval between production of successive drops was held constant at 27.3 ms. This corresponded to a drop-spacing to drop-diameter ratio of 10 for the smallest drops and 75 for the largest drops. Investigations by Cataneo (1970) have indicated a maximum downstream distance of 50–100 drop diameters over which the wake can be detected for drops falling at terminal velocity. In the experiments described here, drop speeds at impact were always less than 50 % and typically 30 % of their terminal velocities, thus the drop separations used guaranteed that wake effects could be ignored. This was not true of the experiments performed by Brazier-Smith *et al.* (1971) where drop separation was of the order of only 2.5 diameters. There remains the problem that drops have not achieved their free fall shape; this effect was not investigated.

Photography of an interaction sequence was facilitated by using backlighting through a diffusing screen, the light source being a gated single-flash xenon tube triggered from a variable delay (2) slaved to the drop generators. A Bolex RX5 H16 cine camera operating in a single-frame advance mode was also activated by delay (2) and was positioned so that the entire interaction (to the point of break-up, if occurring) was in the field of view. The intensity of the illumination was adequate for the use of Plus-X film (50 ASA) with a lens aperture of $f8$; even with the large field of view employed, droplets of radius 50 μm were easily visible. Since the only manual intervention required during filming was the incremental adjustment of delay (2) between each flash, framing rates of better than 1/s were achieved.

For each different impact situation about 12 frames were exposed, the incremental delay being changed by steps of 2 ms. The first two frames consisted of images of the drop pair before contact and were used for the calculation of impact speed, U, and impact parameter, X. The charge induced on the larger drop (by means of a Faraday cylinder) was then changed and a further 12 frames taken as before. The effects of five values of induced charge from zero to about 2×10^{-12} C were filmed in this manner. The sign of the induced charge used was always positive since there is no reason to suspect a sign dependence. The smaller drop always had zero charge, since preliminary experiments indicated that the magnitude of the difference in drop charges influenced the collision rather than the total drop charge. Charge increments were made approximately exponential so that a wide range of charges could be studied. The filming sequence was repeated for each new value of impact parameter, about 13 such sequences (approximately 800 frames) being taken for each of the six drop pairs.

Table 1 gives data on the needles used and the drops they generated. The table gives the inner and outer diameter of each needle, the range of drop radius that could be stably produced, the mean terminal velocity of the drop, V_T, its fundamental period of oscillation, τ_2, the time constant for viscous damping of the oscillations, τ_d, and the average mass, m, of each drop.

Table 2 shows some of the properties of the six possible interactions. The relative terminal velocity, ΔV_T, is calculated from the table given by Mason (1971). The ratio R/r has appeared in

theories of drop instability (see, for example, Brazier-Smith *et al.* 1971), and R_0 is the radius of the resultant drop should coalescence occur. The mass ratio $(r/R_0)^3$ appears in equations describing collisions in the centre of mass (c.o.m.) frame of reference and is also useful in describing the distribution of mass resulting from drop breakup. The parameters e_T and e_R defined earlier are seen to cover the entire region of interest (see also figure 1). Time scales of oscillation and of breakup are indicated by τ_2^0, the period of oscillation of a drop of radius R_0, and by τ_c, the time taken for drops to pass each other. It may be seen that the 2 ms increment used in filming a collision sequence is sufficiently small to allow a detailed study of deformation and rotation, except in the case of glancing collisions with drop A. The rotational energy of the incident drop pair is used to calculate ω_0, the angular frequency of rotation of a rigid sphere of radius R_0, and also to calculate ω_S, the angular frequency of rotation of the dumbell-shaped combination of two rigid spheres of radius r and R. These frequencies indicate the rate at which the combined distorted drop will rotate.

TABLE 1

needle	A	B	C	D
gauge	23	18	14	12
outer diameter/cm	0.061	0.122	0.203	0.264
inner diameter/cm	0.030	0.081	0.152	0.203
drop radius/cm	0.05–0.07	0.09–0.12	0.11–0.16	0.13–0.18
V_T/(m s^{-1})	5.2	6.8	7.7	8.0
τ_2/ms	4.7	9.5	12.9	14.5
τ_d/ms	70	170	260	310
m/mg	1.1	4.1	7.8	10.0

TABLE 2

interaction	AB	AC	AD	BC	BD	CD
r/cm	0.060	0.062	0.058	0.109	0.113	0.142
R/cm	0.097	0.115	0.130	0.153	0.166	0.172
ΔV_T/(m s^{-1})	1.7	2.3	3.1	1.3	1.4	0.6
R/r	1.6	1.9	2.2	1.4	1.5	1.2
R_0/cm	0.104	0.121	0.134	0.170	0.182	0.200
$(r/R_0)^3$	0.19	0.13	0.08	0.26	0.24	0.36
e_T	2.2	2.8	3.2	2.4	2.7	1.6
e_R/X^2	0.91	1.05	0.77	1.45	1.55	0.53
τ_2^0/ms	9	11	13	18	20	23
τ_c/ms	1.8	1.5	1.2	4.0	4.0	5.2
$\omega_0 X^{-1}$/s^{-1}	961	803	601	566	535	268
$\omega_s X^{-1}$/s^{-1}	579	564	487	309	299	131
V/(m s^{-1})	2.7	2.7	2.9	3.1	3.3	3.6
v/(m s^{-1})	1.0	0.7	0.6	2.1	2.2	2.6
Φ	2.5°	1.3°	2.9°	0.6°	2.6°	2.8°
ϕ	−7.0°	−14.3°	−20.7°	−3.2°	−4.0°	−2.6°
U/(m s^{-1})	1.7	2.0	2.4	1.1	1.2	0.9
δ	8°	6°	9°	8°	14°	17°

THE TRANSFORMATION AND REDUCTION OF DATA

The parameters of interest which can be extracted from the data are the impact parameter, X, the sizes and relative velocities of drops both before and after the collision, and the shape-dependent factors A_S and A_R (see equation (I 4)) during an interaction. Quantities which could be obtained directly were the sizes and positions of undistorted drops, the approximate position of the centre of mass, and the length and orientation of the major axis of distorted drops. While

the quantities size and length are reference-frame independent, position and orientation are different in the laboratory and c.o.m. frames. Furthermore, the impact parameter, X, must be measured in the c.o.m. frame and it is therefore desirable to transform all distances and orientations into this frame of reference. If the apparent impact parameter as measured from photographs in the laboratory frame of reference is X_L, then the true impact parameter, X, is given by

$$X = X_L \cos\delta - (1 - X_L^2)^{\frac{1}{2}} \sin\delta,$$

where δ is the angle between the differential velocity vector of the drops and the vertical.

None of the previous investigators has indicated how X was calculated. This is an unfortunate omission, since substantial errors occur if X_L is used instead of X. The discrepancy is largest when the interacting drops have similar fall speeds; in particular, X_L may be of opposite sign to X, indicating drop rotation in the wrong direction. A graph of X as a function of X_L is an ellipse of eccentricity $(1 - \frac{1}{2}\tan^2\delta)^{\frac{1}{2}}$.

Table 2 also shows the speeds and angles measured for the six interactions studied. V and v are the actual speeds of the larger and smaller drop respectively, at the moment of impact, and Φ and ϕ the angles of their individual trajectories to the vertical. The quantity U is the differential speed of the drop pair, so that δ is a calculated quantity given by either of the relations

$$U\cos\delta = V\cos\Phi - v\cos\phi,$$
$$U\sin\delta = V\sin\Phi - v\sin\phi.$$

Measurements were also made of the lengths of the major axes of distorted drops. Although such a measurement only describes the gross features of drop distortion, no more representative measure is available in the absence of a suitable model for asymmetrical shapes.

The experimental errors

The mean and standard deviation of the measurements of incident-drop size were calculated from draughted images. The error varied from 3.8 % to 6.5 % with a mean of 5.2 %. Measurements of drop size are therefore accurate to about 5 %, this error being considerably reduced when grouping (radius classification) and calculation of marginal distributions are performed. The error in the calculation of U and δ was estimated from a number of individual calculations performed for the AB interactions. The standard deviation in U was 3 %, and the error in δ was 14 % or about 1°. Since interactions were classified into five intervals of impact parameter, corresponding to angles of contact of 0° to 90°, the error in δ was not significant. Errors of the order of $\pm 5°$ were inherent in angle of rotation measurements. This was estimated by repeating measurements in an unbiased fashion. Since data were again grouped for display purposes and angles ranged from 0° to 180°, the measurement error was of little consequence. The largest errors were undoubtedly those present in the measurement of distorted drops, though invoking an ellipsoidal assumption reduces this error considerably. The drop sizes resulting from a particular collision were also scaled to conserve mass; this tends to compensate for any systematic error in estimating drop size. As with other data, grouping is useful in limiting the influence of any errors. The method of drop production was sufficiently consistent over 500 interactions that negligible errors through variation of drop size and trajectory were introduced.

PHILOSOPHICAL TRANSACTIONS OF THE ROYAL SOCIETY A MATHEMATICAL, PHYSICAL & ENGINEERING SCIENCES

Discussion of the experimental results

(a) *Rotation of drops after collision*

The angle of rotation (in the c.o.m. frame) is shown as a function of time, t, and of impact parameter, X, for each collision combination, in figure 3; four basic kinds of rotation behaviour were noted:

(i) For low values of X (head-on, or direct collisions) the drop oscillated and rotation was minimal; if breakup occurred the larger product emerged from the base of the unstable drop, and products and satellites formed in a single line.

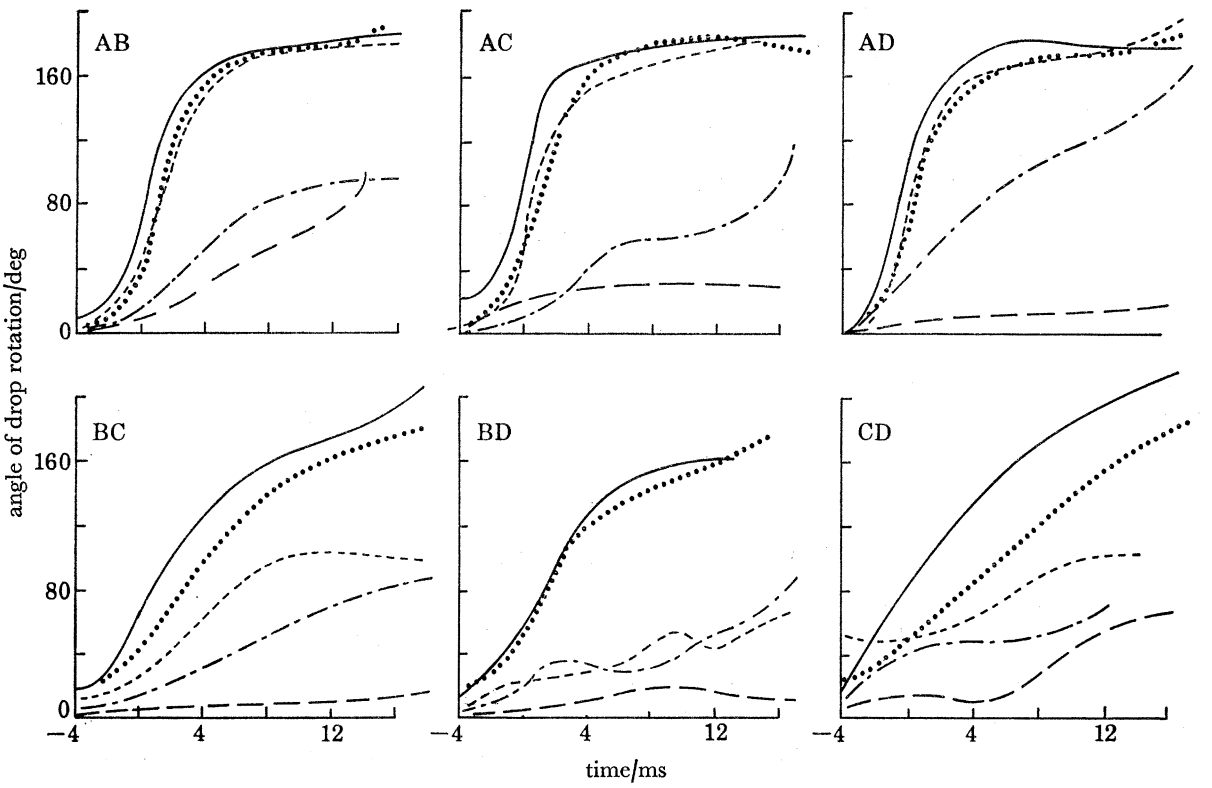

Figure 3. The angle of drop rotation in the centre-of-mass frame as a function of time and the range, j, of the impact parameter, X, for the six interactions studied. Zero time is the moment of contact. ---, $0 < X < 0.2$ ($j = 1$); — — —, $0.2 < X < 0.4$ ($j = 2$); ——, $0.4 < X < 0.6$ ($j = 3$); ·····, $0.6 < X < 0.8$ ($j = 4$); ------, $0.8 < X < 1.0$ ($j = 5$).

(ii) For higher values of X, rotation without breakup was observed to proceed at an almost constant rate; no effects of drop oscillation on the rotation were noted.

(iii) For the intermediate values of X (as in (ii) above), rotation with breakup showed an asymptotic approach to 90°, product drops having similar trajectories to the incident drops.

(iv) For high values of X (grazing contact), either drop rotation or shear generally resulted in breakup. Shear is defined here as contact and breakup with high rotational energies without rigid rotation. Since the angular velocity at contact is significantly different from that of two rigid spheres with the same angular momentum, either drop distortion or disruption must occur to conserve angular momentum. The rate of distortion of drops by capillary waves is limited

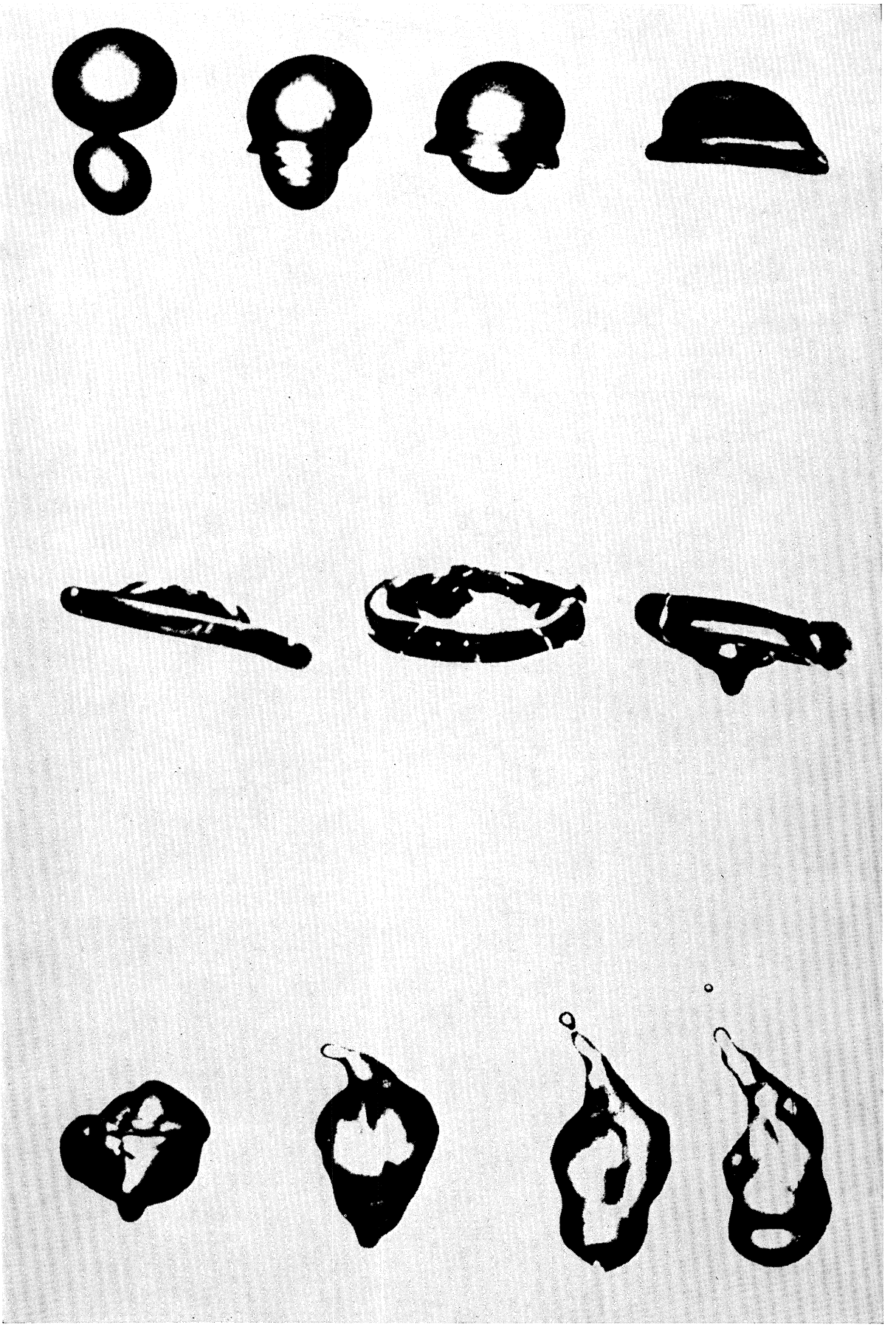

FIGURE 4. A sequence of frames showing the collision of a drop of radius 1.7 mm with one of radius 1.2 mm. The impact parameter, X, is zero. (*Facing p.* 644)

PHILOSOPHICAL TRANSACTIONS OF THE ROYAL SOCIETY A MATHEMATICAL, PHYSICAL & ENGINEERING SCIENCES

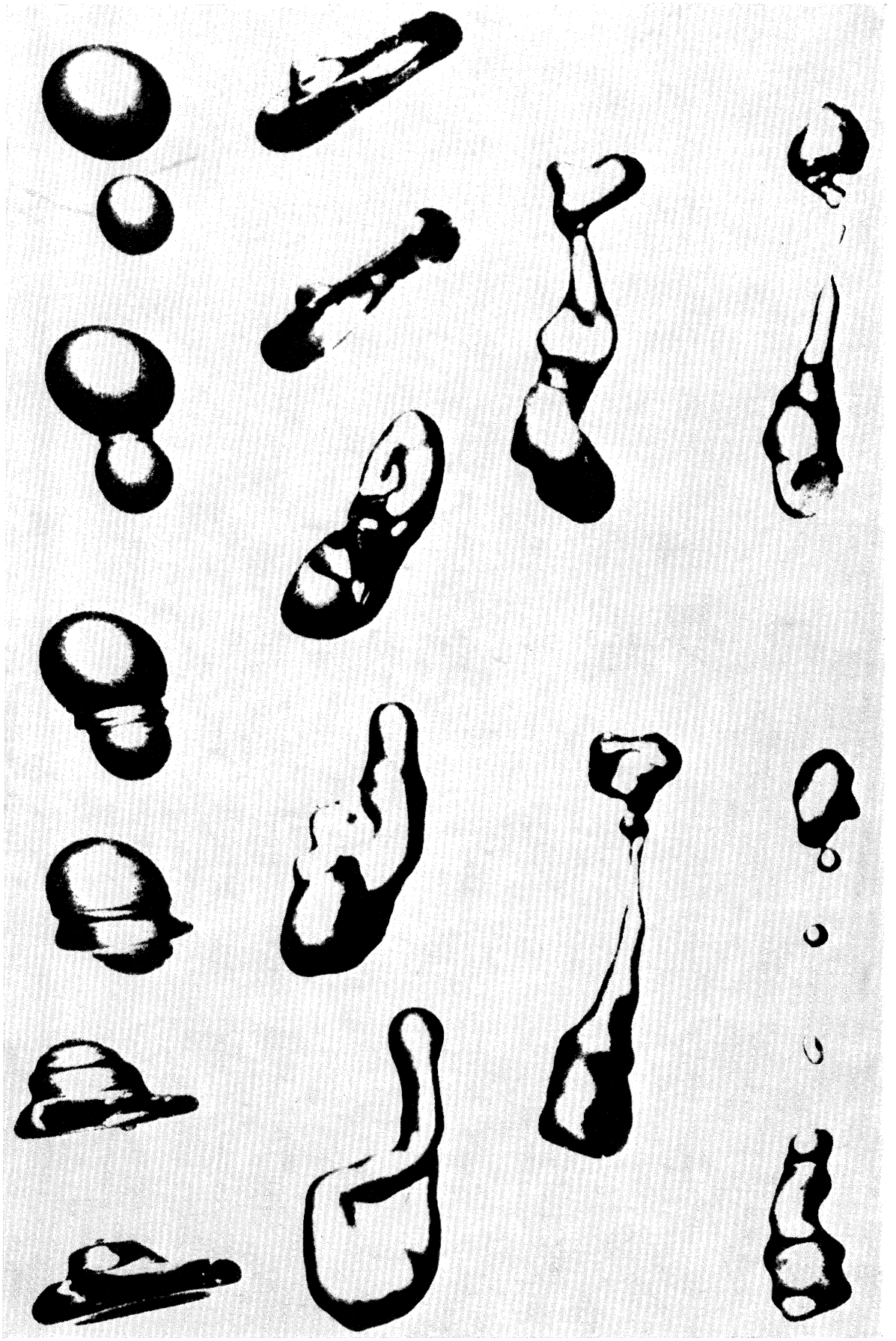

FIGURE 5. As for figure 4 but with the impact parameter, X, set to 0.35. The series exemplifies disruption by rotation.

PHILOSOPHICAL TRANSACTIONS OF THE ROYAL SOCIETY A MATHEMATICAL, PHYSICAL & ENGINEERING SCIENCES

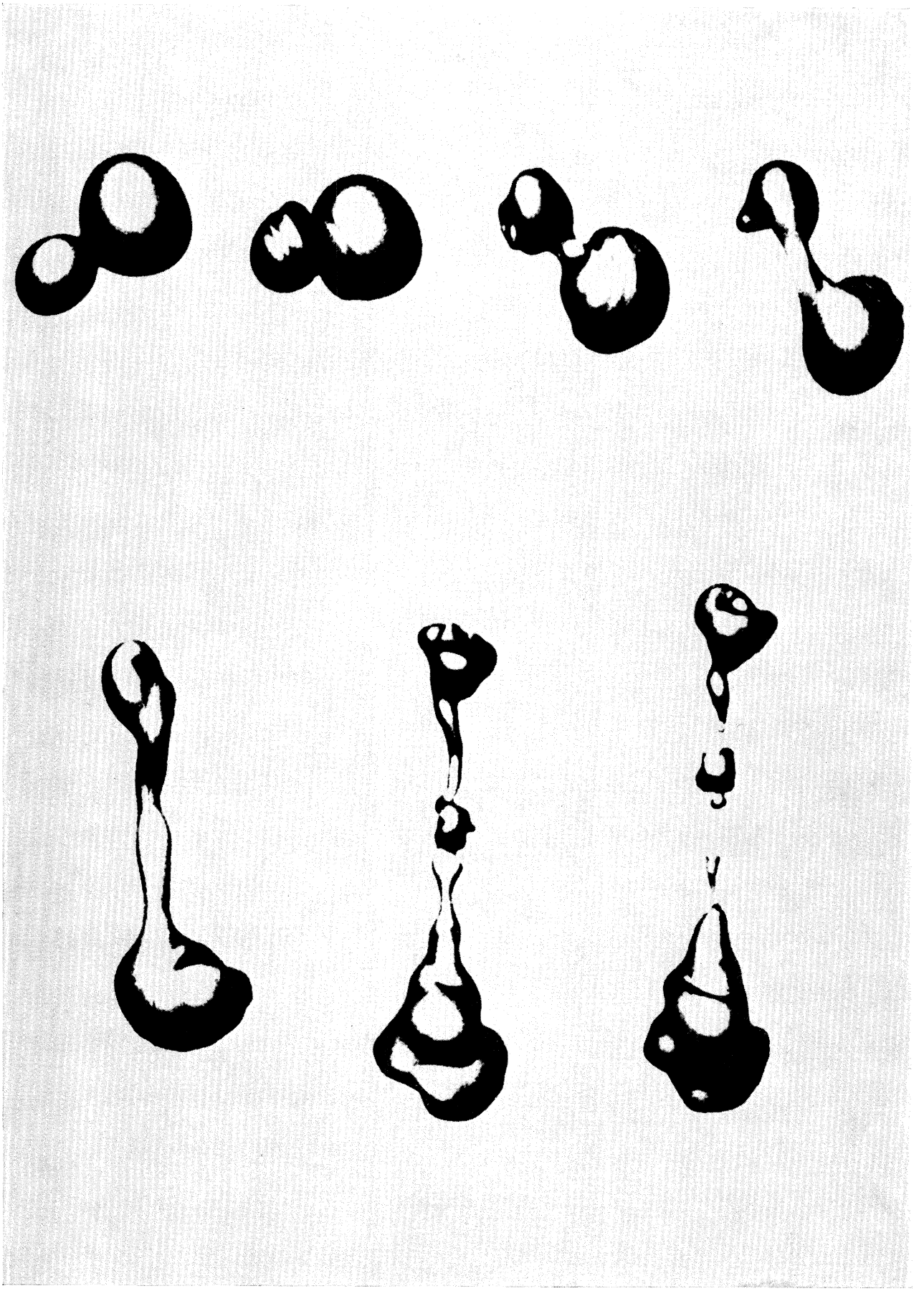

FIGURE 6. As for figure 4 but with the impact parameter, X, set to 0.90. The series shows disruption by a shearing action.

PHILOSOPHICAL TRANSACTIONS OF THE ROYAL SOCIETY A MATHEMATICAL, PHYSICAL & ENGINEERING SCIENCES

(see τ_2^0 in table 2) and so disruption via shear occurs for collisions with high initial rotational energies. For such collisions the reflexion angle, or total rotation after impact, is approximately 180°. Figures 4–6, plates 1–3, show examples of a collision sequence between drops of radius 1.2 mm and 1.7 mm for the cases (i), (iii) and (iv) respectively.

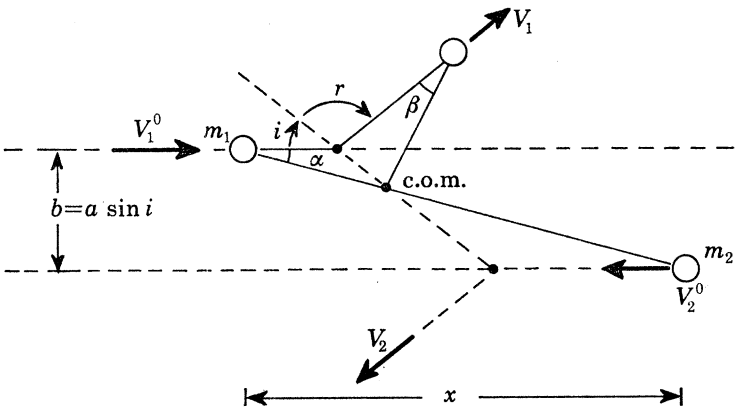

FIGURE 7. The geometry of an inelastic collision between two solid spheres of different size.

Theoretically, the angle of rotation should increase monotonically with time, and summation over a number of interactions should not affect this monoticity. The fluctuations which are to be seen in figure 3 are due to either small differences in the interactions comprising a given sequence, or, more commonly, to the occurrence of contact at a slightly different time; either factor can be expected to cause fluctuations at the end of each curve. The curves of figure 3 were generated from averages over random samples of about 5 collisions for each range of X, with the exception that for the interactions AB the curves for the upper three ranges of X were derived from a much larger sample. As expected, the end fluctuations disappeared. The decrease in the angle of rotation for large t is attributable to the effect of gravity on the drop trajectories. The rates of rotation measured compare favourably with those predicted by the quantities ω_0 and ω_S of table 2, and show clearly the marked decrease to be expected from that for energetic collisions (AB) to that for low-energy collisions (CD).

The shapes of the curves of figure 3 may be compared with those predicted by a model of the inelastic collision between solid spheres. Figure 7 summarizes the conditions before and after collision has taken place in the c.o.m. frame of reference. In the figure, i is the angle of incidence at the moment of collision, t_C, and r is the angle of reflexion; the quantity, a, is the sum of the radii of the impacting spheres.

$$\cot\alpha-\cot i=(V_1^0-V_2^0)\,(t-t_C)/a\sin i \quad |t<t_C|, \tag{I 6a}$$

$$\cot\beta-\cot r=(V_1-V_2)\,(t_C-t)/a\sin r \quad |t<t_C|, \tag{I 6b}$$

where $\beta=i+r-\alpha$, and the coefficient of restitution, e, is introduced through the equations $\cot r=e\cot i$ and $(V_1-V_2)=(V_1^0-V_2^0)\,(\sin^2 i+e\cos^2 i)^{\frac{1}{2}}$.

Figure 8 shows a plot of equation (I 6) with the quantity α as ordinate, and the quantity $(V_1-V_2)\,(t-t_C)/a$ as the abscissa. Curves are shown for selected values of the angle of incidence, i, and coefficient of restitution, e; they show a marked resemblance to the experimentally derived curves of figure 3.

When breakup occurs, there is opportunity for the separation of charge between the drop products. Many workers have discussed these electrical effects and it clear that the majority of charge separating mechanisms are sensitive to the electric field vector during collision and breakup. Their arguments indicate that the orientation of the two-drop system is equally important, yet experiments to investigate charge exchange (such as those of Jennings & Latham (1971)) have ignored this effect. The angle of the axis of the distorted drops to the vertical demonstrates a marked difference in the behaviour of low energy collisions and high energy collisions. For the collisions AB, AC and AD this angle never exceeded 10° whatever the value of X. On the other hand, angles greater than 40° proved possible for moderate and large values of X for collisions BC, BD and CD. The implications of these data in the context of charge-exchange theory will not be discussed here.

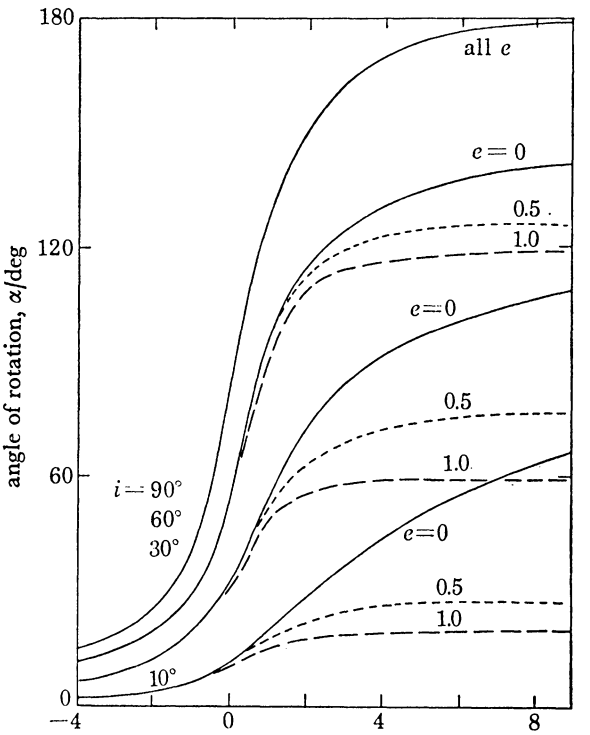

FIGURE 8. The variation with time of the angle α between the centres of two rigid spheres and their initial line of motion. Curves are shown for selected values of the angle of incidence, i, and of the coefficient of restitution, e.

(*b*) *Charge-dependent distributions*

Neither the rotation of the two-drop system nor its mechanical distortions were found to be at all sensitive to electrical charge, which was therefore discarded as an input parameter. However, certain distributions describing important properties of the products of collision were found to be charge-dependent and are discussed below. The values of the charge, Q_K, placed upon the larger drop of a given pair of drops are given in table 3 together with the calculated value of the charge parameter e_C of equation (I 5). These values of charge are referred to below in terms of the index, K, which varies as an integer from 0 to 5 for each interaction. The upper limit of charge was chosen to not exceed that usually found on atmospheric precipitation.

(*c*) *Product radii for energetic collisions*

Drop sizes were classified according to equal-width radius-ratio intervals; that is, according to the ratio r/R_0. This device facilitated the comparison of data from the different interaction groups. Since drops were somewhat distorted following breakup, the radius of the equivalent sphere for each drop was calculated assuming that the drops were ellipsoids of revolution. This method required the measurement, therefore, of both the major and minor axes of each drop and was used for all but the smallest products. The orientation of a drop and its behaviour after breakup allowed an unambiguous determination of whether a given drop was prolate or oblate; deviations from the ellipsoidal shape were common.

TABLE 3

		index K				
interaction	parameter	1	2	3	4	5
AB	$Q_K \times 10^{-12}$ C	0	0.13	0.27	0.54	1.08
	$e_C \times 10^{-8}$	0	4	14	57	230
AC	$Q_K \times 10^{-12}$ C	0	0.16	0.32	0.64	1.28
	$e_C \times 10^{-8}$	0	3	14	55	221
AD	$Q_K \times 10^{-12}$ C	0	0.18	0.36	0.72	1.44
	$e_C \times 10^{-8}$	0	3	13	51	206
BC	$Q_K \times 10^{-12}$ C	0	0.21	0.43	0.85	1.70
	$e_C \times 10^{-8}$	0	2	9	34	137
BD	$Q_K \times 10^{-12}$ C	0	0.23	0.46	0.92	1.84
	$e_C \times 10^{-8}$	2	8	34	134	536
CD	$Q_K \times 10^{-12}$ C	0	0.19	0.38	0.76	1.52
	$e_C \times 10^{-8}$	1	4	17	69	276

The charge marginal frequencies (i.e. those summed over all X for a given drop charge) of drop radius ratio are given for the interactions AB, AC and AD in figure 9. Coalescences are included as a narrow spike with unit radius ratio. Distributions were found generally to be tri-modal with two of the modes corresponding roughly to the radius ratios for the incident drops (shown as dotted lines), and the remaining mode at low values of radius ratio attributable to so-called satellite drops. The presence of the latter mode was not evident from a visual examination of photographs; in this respect the use of equal-width radius-ratio intervals proved fortuitous.

The mode of the largest products was found to be distinct from the other two and has a peak very close to that of the larger incident drop. On the other hand the position of the central mode corresponded to a somewhat smaller radius than that of the smaller incident drop, and suggests that some of the mass of the smaller drop is transferred both to the larger incident drop and to the satellite drops. (The total mass of satellites did not exceed 10 % of the total mass on any occasion.) While there were clear differences between the distributions for the collisions AB, AC and BC, the effects of variation in drop charge were slight.

Impact parameter marginal distributions (i.e. those summed over all K for a given X) for the collisions AB, AC and AD are shown in figure 10. The form of the distribution is similar to that for the charge margins. As before, the shift of the central peak with an increasing energy of collision was evident, but the shift was found to diminish with an increase in the impact parameter X. These data suggest that the mass loss of the smaller drop is greater for direct

collisions where a higher degree of drop contact and mixing is possible. A further effect to be noted is that the peaks of each distribution became narrower as the value of X was increased.

Overall radius-ratio distributions are shown in figure 11 for the interactions AB, AC and AD. Here it shows clear evidence of the shift of the central peak with increasing energy of the collision, the shift coinciding with a narrowing of the distribution of the largest products.

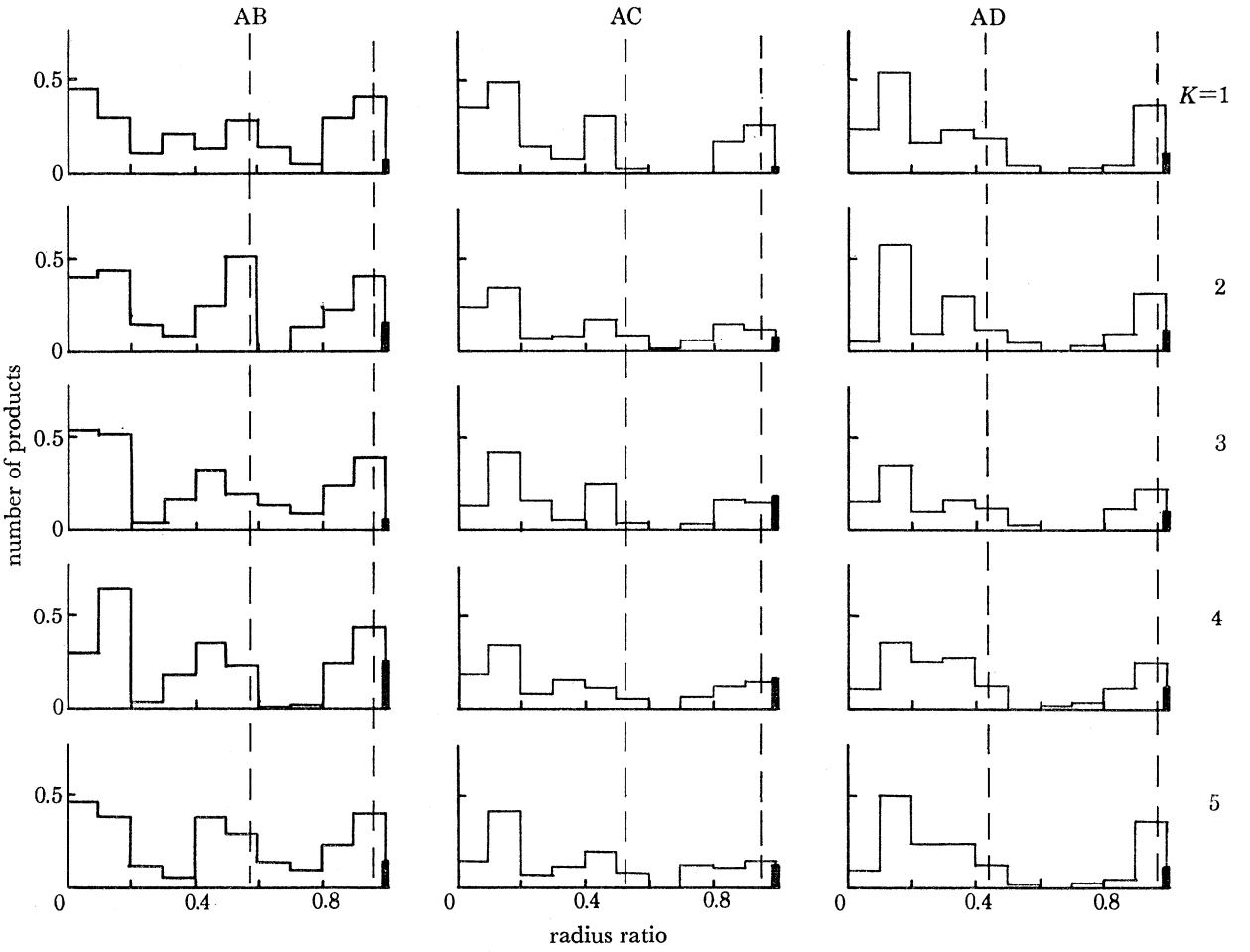

FIGURE 9. Charge marginal distributions of the number of drop products per radius-ratio interval and per collision as a function of the drop radius ratio. The charge index, K, is defined in table 3. The dashed lines indicate the radius ratios of the incident drops.

(*d*) *Distributions of mass and mass transfer in a two-body system*

Since few satellites were produced by the collisions BC, BD and CD, these interactions were amenable to comparison with the following simple theoretical model.

In many cases, drop collisions result in the formation of large product drops, similar in size to the incident drops, plus several very much smaller satellite drops. In such instances the distribution of product-drop mass can then be treated separately from the distribution of satellites. The only previous investigations of product-drop size have been those of List, MacNeil & McTaggart-Cowan (1970) and McTaggart-Cowan & List (1975). They noted that products were distributed as two superimposed Gaussian curves centred on the radii of the impacting

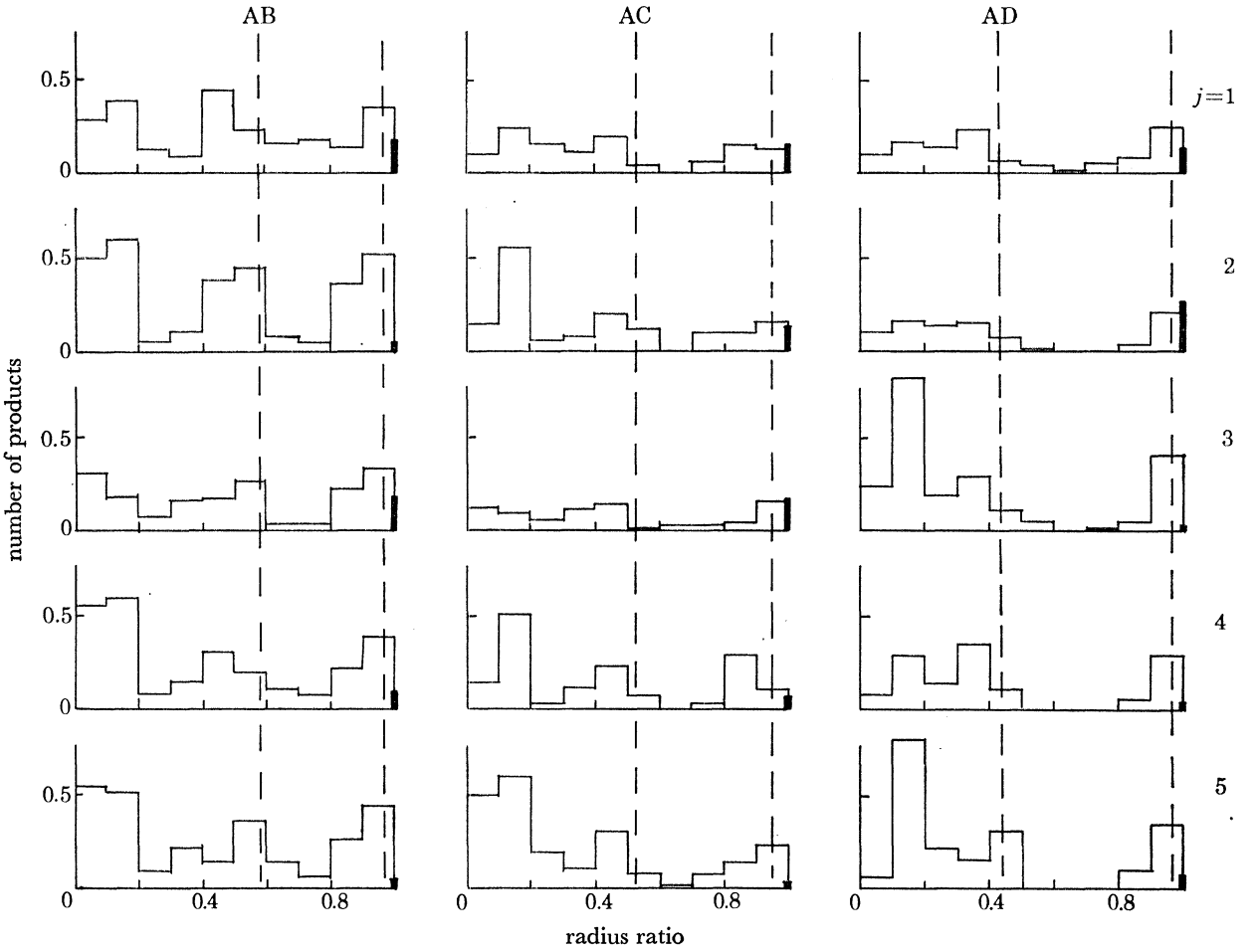

FIGURE 10. Impact parameter marginal distributions of the number of drop products per radius-ratio interval and per collision as a function of the drop radius ratio. The impact parameter index, j, is defined in the legend of figure 3. The dashed lines indicate the radius ratios of the incident drops.

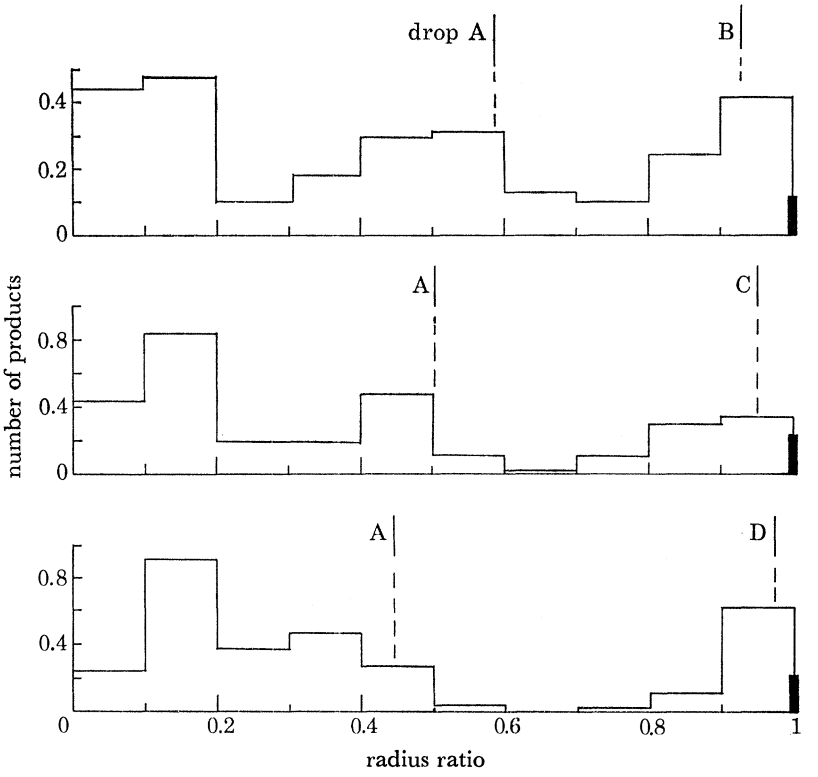

FIGURE 11. The overall distribution of the number of drop products per radius-ratio interval and per collision as a function of the drop radius ratio. The incident drop radii are indicated by the dashed lines.

drops. While this describes the general form of product distributions, it neglects a fundamental relation, namely that the masses of the two drops formed as the major products, m_1 and m_2, must satisfy the condition

$$m_1 + m_2 = M_0,$$

where M_0 is essentially the combined mass of the incident drops.

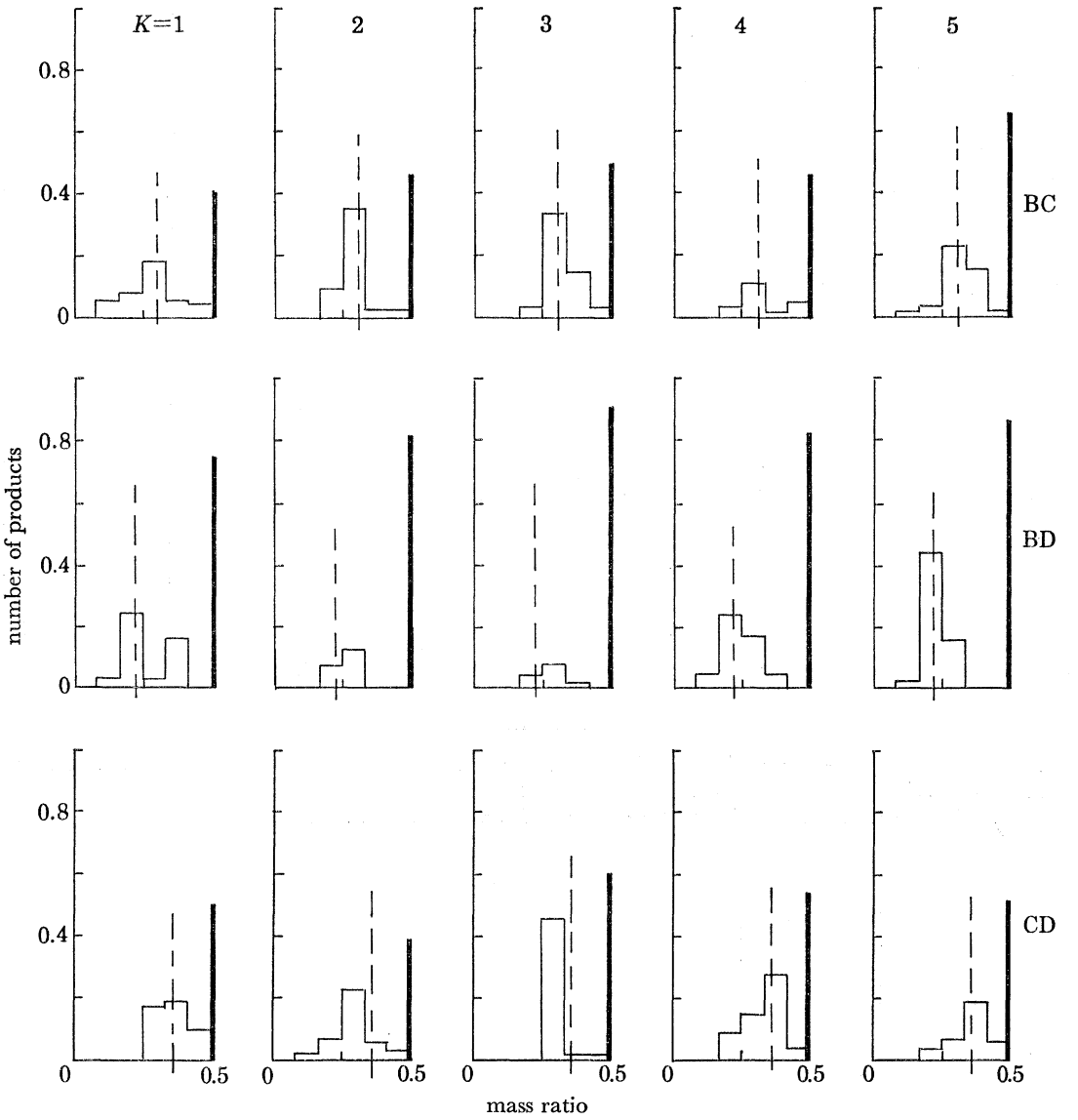

FIGURE 12. The charge marginal distribution of the frequency of production of lone drop pairs of a given mass ratio for the interactions BC, BD and CD. The dashed line shows the mass ratio of the incident drops.

If the overall mass distribution, $\Psi(m)$, is considered to consist of two superimposed distributions, $\psi_1(m)$ and $\psi_2(m)$, arising from pairs of drops of mass m_1 and m_2 respectively, then

$$\Psi(m) = \psi_1(m) + \psi_2(m).$$

It is convenient to compare interactions by normalizing m with respect to M_0, so that if $m/M_0 = x$, then since drops are produced in pairs

$$\Psi(x) = \psi(x) + \psi(1-x).$$

A distribution which nearly satisfies the conditions $\Psi(x=0)=\Psi(x=1)=0$ and agrees well with the observations of List *et al.* (1970) and with the results of the experiments described here is

$$\Psi(x) = (1-E)\,(2\pi)^{\frac{1}{2}}\sigma\,[\exp\{-\tfrac{1}{2}(x-\mu)^2/\sigma^2\}+\exp\{-\tfrac{1}{2}(x-1+\mu)^2/\sigma^2\}].$$

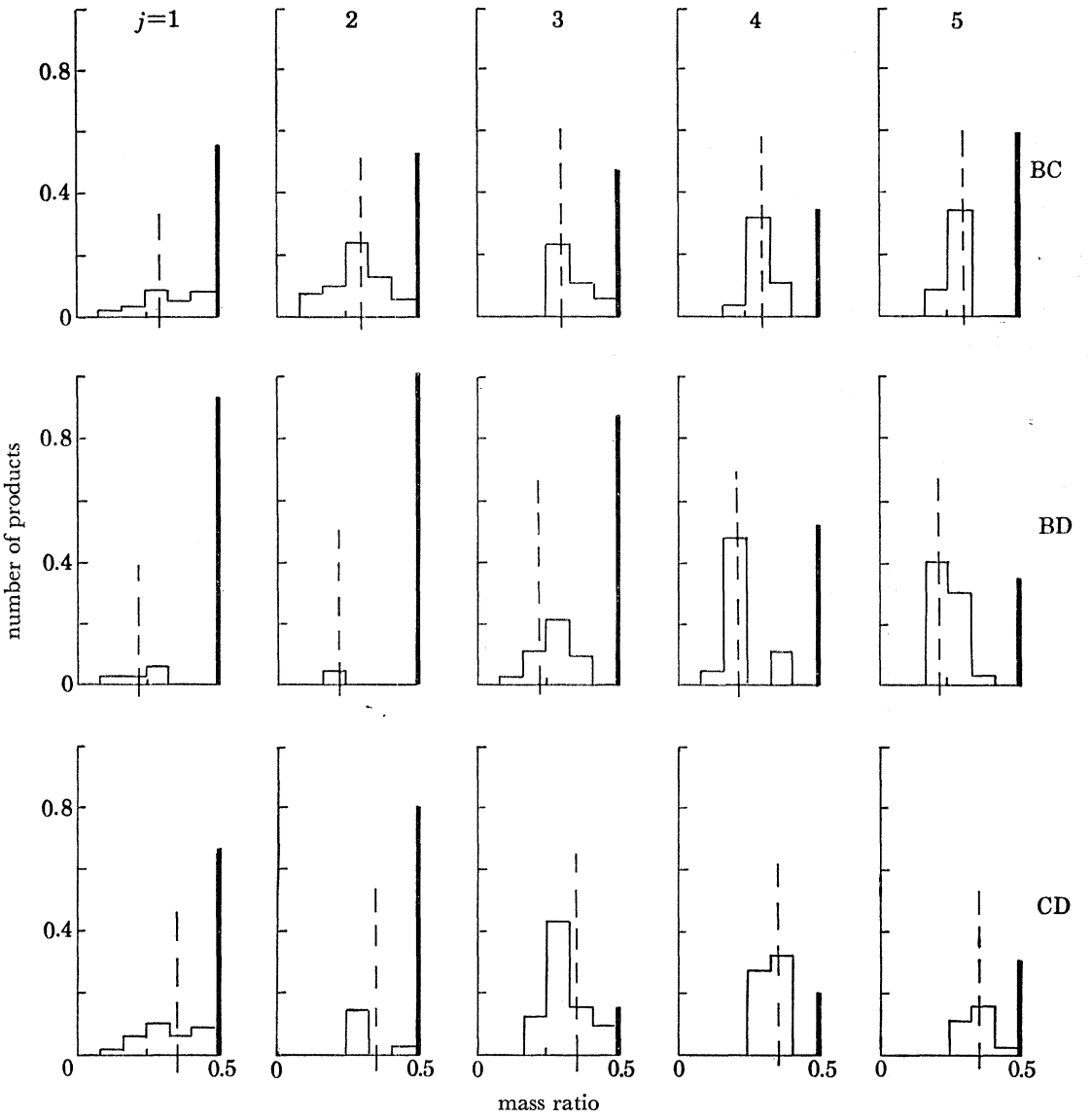

FIGURE 13. The impact parameter marginal distribution of the frequency of production of lone drop pairs of a given mass ratio for the interactions BC, BD and CD. The dashed line shows the mass ratio of the incident drops.

Charge marginal distributions of mass ratio are shown in figure 12; only half of the symmetrical distribution has been plotted. The distribution is essentially unimodal, with a peak close to the value of the mass ratio of the incident drops. The mean and standard deviations μ and σ of each distribution were found from the second and fourth moments of $\Psi(x)$. These data appear in table 4. In contrast, the impact parameter marginal distributions shown in figure 13 show a marked dependence upon the impact parameter, X. The distribution is narrower for glancing

TABLE 4

charge marginal distribution (see figure 12)	interaction BC μ	BC σ	BD μ	BD σ	CD μ	CD σ
$K = 1$	1.07	0.34	1.11	0.32	1.00	0.16
$K = 2$	1.09	0.17	1.08	0.17	0.81	0.19
$K = 3$	1.18	0.19	1.15	0.20	0.83	0.06
$K = 4$	1.21	0.27	1.02	0.26	0.93	0.21
$K = 5$	1.19	0.33	0.95	0.16	1.01	0.21
impact parameter marginal distribution (see figure 13)						
$j = 1$	1.27	0.38	1.01	0.31	0.91	0.28
$j = 2$	1.10	0.36	0.87	0.01	0.86	0.11
$j = 3$	1.25	0.18	1.18	0.29	0.87	0.18
$j = 4$	1.14	0.17	0.95	0.23	0.93	0.12
$j = 5$	1.04	0.14	1.03	0.18	0.97	0.13

The quantities μ and σ have been normalized to permit comparisons by dividing actual values by $[r^3/R^3+r^3]$ ($= 0.2656$ for BC; 0.2398 for BD; 0.3600 for CD).

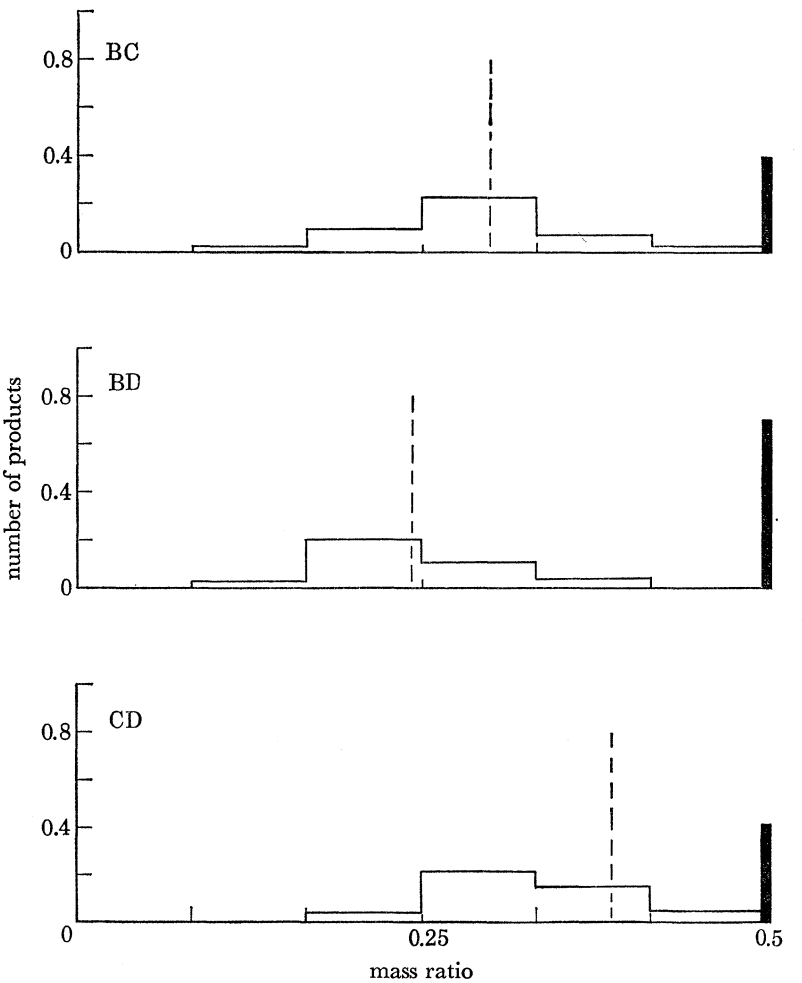

FIGURE 14. The overall distribution of the frequency of production of lone drop pairs of a given mass ratio for the interactions BC, BD and CD. The dashed line shows the mass ratio of the incident drops.

collisions than for direct collisions (this conclusion was confirmed by statistical tests not shown here). No impact energy dependence is evident in these distributions.

However, consideration of the overall distributions of mass, given in figure 14, does suggest a dependence on the energy of the impact that is not otherwise apparent. There is a clear shift of the distribution mode away from the value of incident-drop mass ratio as the impact energy decreases; such a trend indicates an increase in mixing and mass exchange.

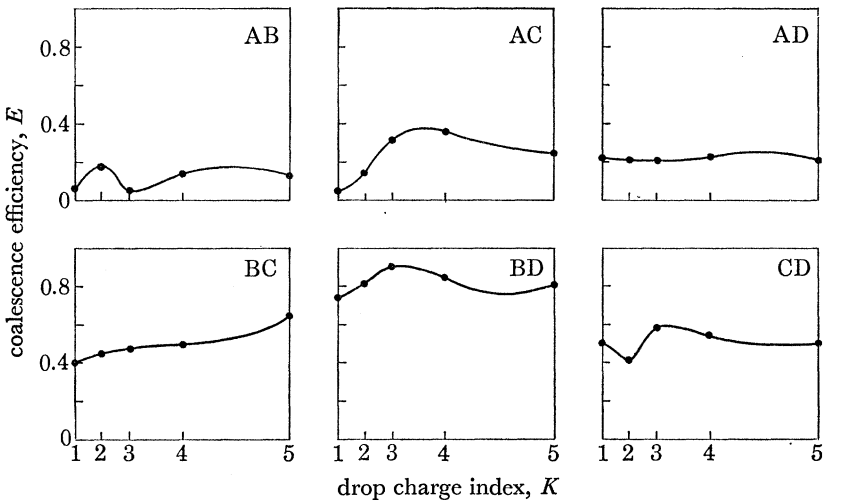

FIGURE 15. The variation of drop coalescence efficiency, E, with charge index, K, for the six interaction types studied.

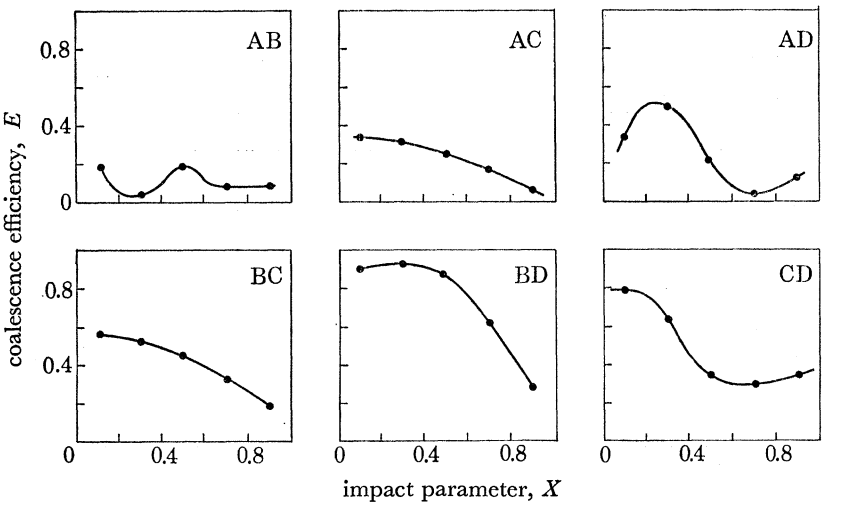

FIGURE 16. The variation of drop coalescence efficiency, E, with impact parameter, X, for the six interaction types studied.

(e) *The frequency of coalescence*

The effects of electric charge, Q, and the impact parameter, X, were investigated with the aid of figures 15 and 16. Coalescence frequency generally decreased with increasing impact parameter, although for the collisions AC, AD and CD, there is a peak in coalescence frequency at an intermediate value of X. The dependence upon drop charge varied less predictably with

collision type, thus collisions AD, BD and CD show very little dependence upon drop charge, whereas a slight dependence is evident for collisions BC.

When drops were charged the collisions AB and AC exhibited an enhanced coalescence frequency. Also coalescence frequency was higher for the low-energy collisions.

Summary

A suitable set of parameters has been defined to describe a two-drop interaction. The set comprised the quantities: total charge, angular momentum, and total energy, and these could be normalized in a convenient way to compare interactions. The range of the parameter values defined was limited to those likely to occur in atmospheric precipitation and it was noted that previous investigations have, unfortunately, not adequately covered the contingencies. The influence of drop charge on the collision dynamics was found to be negligible.

Measurements of product drop sizes have been made which result from interactions of interest in the theories of the generation of raindrop spectra. Coalescence efficiencies have been obtained by statistical treatments which accord with naturally occurring collisions; these data are in contrast to previous experiments by other workers where a model of breakup has been necessary.

The effect of drop charge and impact parameter have been investigated separately and serve to yield the first qualitative evidence of the effect of drop charge upon a wide range of collision types. Nevertheless, the discussion of the results serves only to outline the gross features of the data. Theories of air film stability and the electrohydrodynamic stability of water drops are discussed in parts II and III.

II. AN INVESTIGATION OF AIR FILM STABILITY AND DRAINAGE BETWEEN COLLIDING, ELECTRICALLY CHARGED DROPS

A theory is developed for the rate of expulsion of the viscous layer trapped between colliding drop surfaces. The theory allows for general interface movement and reduces to the classical cubic film-thinning equation when the interfaces are rigid, finite, parallel disks. It is shown that colliding drop surfaces will generally have a time-dependent curvature, and an expression for that curvature is derived. A simple analytical treatment of drop deformation agrees well with more complex numerical treatments and with experiment. Equations are normalized so that drop deformation may be evaluated as a function of time for any pair of equally sized drops provided the Weber number is specified. The generalized thinning equation is integrated together with the drop deformation equations and the surface curvature equation, enabling a critical Weber number for drop coalescence to be determined. The requirement for coalescence of neutral water drops colliding in air is given approximately by $R \leqslant \frac{1}{4}(3We+1)$, where R is a drop radius in millimetres and We is the Weber number.

Enhanced film thinning when drops are charged cannot be explained by the deformation and acceleration of approaching drop surfaces: electrostatic forces between parallel interfaces are found to be very small. A theory for the stability of oscillating charged surfaces predicts drop electrification criteria having the correct form and agreeing to within an order of magnitude with observations.

Introduction

Many workers, for example, Gillespie & Rideal (1956), Charles & Mason (1960), McKay & Mason (1963) and Hartland (1967), have shown that the delay between the impact of two drops and the formation of a liquid bridge joining them is attributable to a viscous film composed of the surrounding medium. This layer separates adjacent drop surfaces and thins slowly until a critical thickness of between 500 Å† and 100 Å is reached. Hodgson & Lee (1969) have shown that Van der Waals' forces overcome electrical double-layer repulsion at this separation and rapid rupture of the film ensues. Delay times for water drops colliding in air have been measured by Owe Berg, Fernish & Gaukler (1963), Jayaratne & Mason (1964) and by Nelson & Gokhale (1973). Results were contradictory with respect to the influence of drop impact speed, although all experiments indicated a strong dependence of delay times on electrical forces. Jayaratne & Mason found that for droplets of greater than 125 μm radius colliding with a plane water surface there was a critical impact speed above which coalescence would occur and below which bouncing took place. Coalescence occurred more readily if droplets were charged or if an electric field was applied. Gunn (1965*b*) found that bounce occurred at impact speeds of less than 0.4 m s^{-1} for pairs of drops of 1 mm radius, and that an applied field of 4×10^3 V m^{-1} guaranteed coalescence. Sartor & Abbott (1968) observed collisions between water drops of 400 and 375 μm radius. Coalescence always occurred for impact speeds of less than 0.21 m s^{-1} and for speeds greater than 0.35 m s^{-1}. Between these limits bouncing always occurred unless suppressed by a field exceeding 2.5×10^3 V m^{-1} or by the drops carrying equal and opposite charges in excess of 6×10^{-14} C. In a later experiment, Sartor & Abbott (1972) examined collisions between drops of equal size with radii in the range 100–800 μm. Drops of radius less than 250 μm always coalesced because the high surface tension forces limited flattening of drop surfaces on impact and air could be forced from between the drops more readily. For larger drops, coalescence occurred at either low speeds (with long contact times allowing completion of film drainage) or at high speeds (with correspondingly large forces to expel the air). Impacts at intermediate speeds resulted in bounce.

The present paper seeks to explain the above observations by combining theories of film drainage, drop distortion, and electrical influence. Discussion is limited to the direct impact between drops of equal size, although some of the results may be extended to other situations.

The theory of squeeze film drainage

(*a*) *Interfaces with fixed profiles*

In an investigation of the lubrication of bearings, Reynolds (1886), derived a single differential equation relating pressure, interface velocities, and film thickness. This approach has not been applied in recent investigations of the drop collision problem but will be used here. The form of Reynolds's equation which is applicable to symmetric collisions between drops is

$$\frac{1}{r}\frac{\partial}{\partial r}\left[h^3 r \frac{\partial}{\partial r}\right] = 12\mu\left\{\frac{1}{r}\frac{\partial}{\partial r}(r u_s h) + \frac{\mathrm{d}h}{\mathrm{d}t}\right\}, \qquad \text{(II 1)}$$

where the position of the interface is defined by $z = h$, p is the pressure within the film, μ is the coefficient of kinematic viscosity within the film medium, and u_s is the radial velocity of the interface. The derivation of this equation assumes that the mean molecular path in the film is

† 1 Å = 0.1 nm = 10^{-10} m.

much smaller than the film thickness; this assumption is valid for the early rate-determining part of the film drainage process. Equation (II 1) is first integrated to obtain $p(r)$. Equating the force F on each drop surface to the integral of $p(r)$ over the area of that surface gives

$$F = -\frac{3\pi\mu a^4}{2h^3}\frac{\mathrm{d}h}{\mathrm{d}t} - \frac{24\pi\mu}{h^2}\int_r^a \left(\int_0^a u_s \,\mathrm{d}r\right) r\,\mathrm{d}r. \tag{II 2}$$

Equation (II 2) is equivalent to that derived by Murdoch & Leng (1971) who assumed that the radial velocity u_s is confined to a region within the drop and close to the surface. Using a second-order theory they found that the expression for the thinning rate involved terms in h^2. On the other hand, Foote (1971) assumed that u_s was proportional to r under which condition equation (II 2) reduces to the form

$$\mathrm{d}h/\mathrm{d}t = -2Fh^3/(3\pi\mu a^4) - 2u_s(a)h/a. \tag{II 3}$$

Experimental observations have not substantiated either model for the drop surface velocity, and no realistic theoretical arguments exist for their support.

(*b*) *Interfaces with time-dependent curvature*

In the models described above it is assumed that the film interfaces are plane, parallel disks. In practice, however, the film near the point of drop impact will have thinned substantially more than the disk edges. The shape of the adjacent drop surfaces is therefore coupled to the rate of flattening of the drops, and the consequent interface curvature enhances film thinning because of the reduced tangential stress.

If the radius of curvature of the interface is given by $\eta(t)$, then for a disk radius $a \ll \eta$ the film thickness is well represented by the parabolic profile

$$h = h_0 + r^2/\eta, \tag{II 4}$$

where h_0 is the film thickness at the axis of symmetry. The radial surface speed u_s, is found by requiring equation (II 4) to represent the interface at all times. Integration of equation (II 1) now yields

$$\frac{\mathrm{d}h_0}{\mathrm{d}t} = -\frac{2Fh_0^3}{3\pi\mu a^4}\left(1 + \frac{a^2}{\eta h_0}\right) - \frac{h_0}{\eta}\frac{\mathrm{d}\eta}{\mathrm{d}t}. \tag{II 5}$$

Equation (II 5) has the same form as equation (II 3) with a term linear in h_0 dominating the right hand side for small film thickness. There is a firm physical basis for the derivation of equation (II 5).

Drop deformation

The deformation of impacting drops has been studied numerically by Foote (1975), but this complicated treatment gives little insight into the physical processes involved. With the same coordinate system as in the previous section, the acceleration of the drop centre of mass, z_0, is approximately

$$\mathrm{d}^2z_0/\mathrm{d}t^2 = p\pi a^2/M, \tag{II 6}$$

where M is the mass of the drop. For small interface curvatures the film pressure p is closely approximated by the drop internal pressure. This is substantiated by the calculations of the pressure field by Foote (1975). Equation (II 6) may therefore be written as

$$\mathrm{d}^2z_0/\mathrm{d}t^2 = 3Ta^2/2\rho R^4, \tag{II 7}$$

where T is surface tension, and R is the radius of the drop of density ρ. An examination of the photographs of drop shapes obtained by Bradley (1975) and discussed in part I of this paper suggests that the distance from the drop centre to the edge of the disk is approximately equal to R throughout the collision and therefore

$$z_0^2 + a^2 = R^2. \tag{II 8}$$

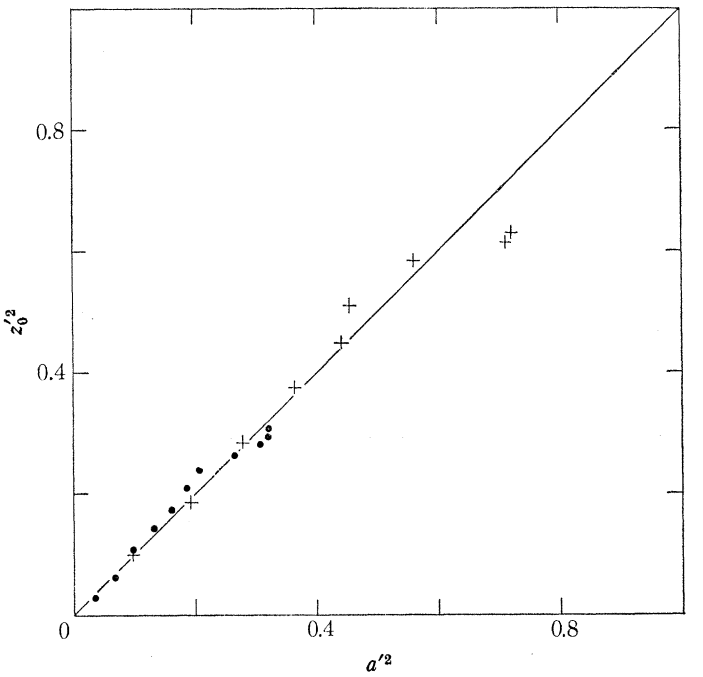

FIGURE 17. A test of the linear relation between normalized square of the centre of mass coordinate, $z_0'^2$, and the normalized square of the film interface radius, a'^2. Data points are derived from Foote (1975). ●, $We = 0.16$; +, $We = 1.42$.

The accuracy of equation (II 8) is confirmed in figure 17, where a plot of $(z_0/R)^2$ against $(a/R)^2$ derived from data published by Foote (1975) has the expected linear form; it should be noted that a different linear relation is followed after the maximum drop distortion has been achieved. Equations (II 7) and (II 8) may be normalized by writing

$$z_0' = z_0/R, \quad a' = a/R, \quad t' = \omega t/2\pi,$$

where

$$\omega = (8T/\rho R^3)^{\frac{1}{2}}$$

is the angular frequency of the fundamental free oscillation mode of a drop of radius R. The resulting differential equation is

$$\mathrm{d}^2 z_0'/\mathrm{d}t'^2 = \tfrac{3}{4}\pi^2(1 - z_0'^2). \tag{II 9}$$

At $t = 0$ the drop centre of mass approaches the origin with speed V_d and hence

$$\begin{aligned} \mathrm{d}z_0'/\mathrm{d}t' &= -2\pi V_\mathrm{d}/\omega R \\ &= -\tfrac{1}{2}\pi(2\rho R V_\mathrm{d}^2/T)^{\frac{1}{2}} \\ &= -\tfrac{1}{2}\pi We^{\frac{1}{2}}, \end{aligned} \tag{II 10}$$

where We is the Weber number for the collision. The initial conditions are therefore

$$z_0' = 1, \quad \mathrm{d}z_0'/\mathrm{d}t' = -\tfrac{1}{2}\pi We^{\frac{1}{2}} \quad \text{at} \quad t' = 0. \tag{II 11}$$

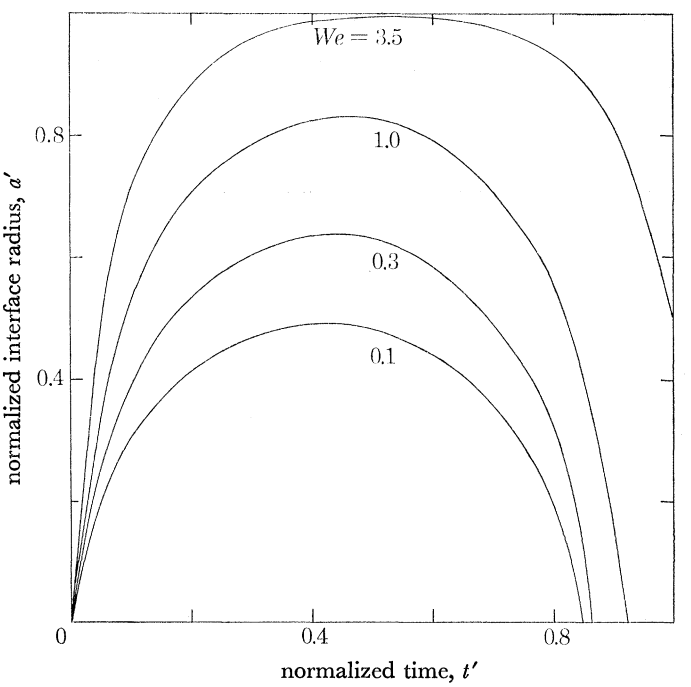

FIGURE 18. The variation of normalized interface radius with time for various selected values of the Weber number *We*.

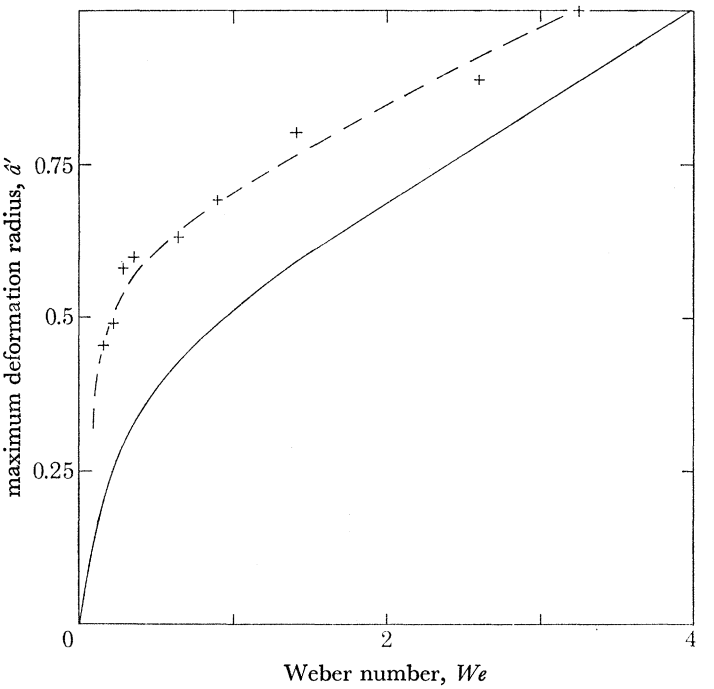

FIGURE 19. The variation of maximum deformation radius, $\hat{a}'$ with Weber number. ——, Theoretical curve; −+−, value derived numerically by Foote (1975).

PHILOSOPHICAL TRANSACTIONS OF THE ROYAL SOCIETY A MATHEMATICAL, PHYSICAL & ENGINEERING SCIENCES

Equation (II 9) may readily be integrated by using a fourth-order Runge-Kutta method and a' derived from equation (II 8); the results are plotted in figure 18.

The curves for figure 18 agree well with those of Foote (1975) for times prior to maximum deformation, although for longer times drop distortion is overestimated for large *We* and underestimated for small *We*. The maximum radius of deformation is plotted as a function of the Weber number in figure 19.

TABLE 5. TYPICAL VALUES OF PARAMETERS IN THE WATER-IN-AIR SYSTEM

		typical value
Thickness	h	10^{-6} m
Interface radius	a	2×10^{-4} m
Pressure	p	10^{3} N m^{-2}
Radial velocity	u	2×10^{-1} m s^{-1}
Normal velocity	v	10^{-3} m s^{-1}
Viscosity	μ	1.7×10^{-5} N s m^{-2}
Force	F	10^{-4} N
Density	ρ	10^{3} kg m^{-3}
Surface tension	T	7.2×10^{-2} N m^{-1}
Radius of curvature	η	2×10^{0} m
Reynolds number	*Re*	10^{-2}
Weber number	*We*	5×10^{-1}

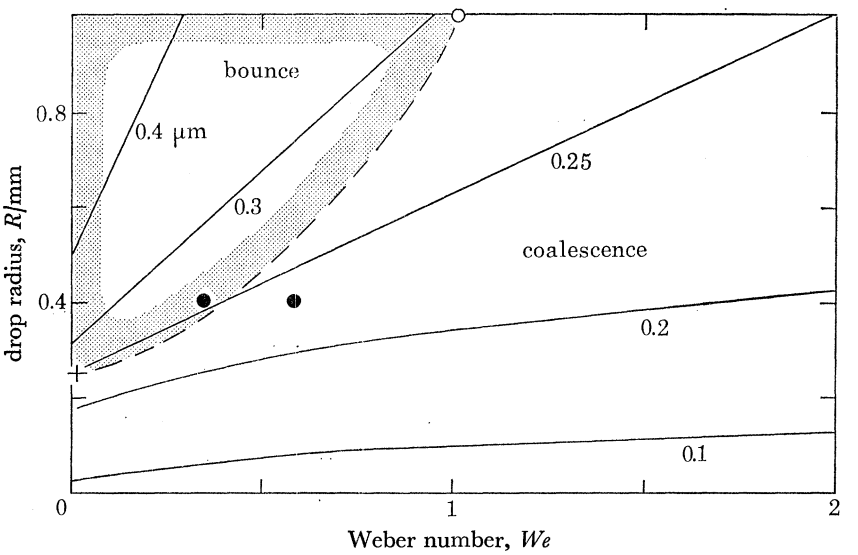

FIGURE 20. Comparison of the theoretically predicted minimum film thickness (solid lines) with experimental observations of the limiting Weber number required for coalescence. ○, Gunn (1965); ●, Sartor & Abbott (1968); +, Sartor & Abbott (1972).

INTEGRATION OF THE THINNING EQUATIONS

Equation (II 5), which describes the rate of change of film thickness with time, may be integrated to obtain a relation between film thickness and time provided R, η, and $\mathrm{d}\eta/\mathrm{d}t$ can be calculated. The force acting on a drop is the product of drop mass and the centre of mass acceleration given by equation (II 9). If the edge of the disk is defined as a region of constant thickness $h-h_0$,

$$\mathrm{d}(h-h_0)/\mathrm{d}t = 0 = 2\frac{a}{\eta}\frac{\mathrm{d}a}{\mathrm{d}t} - \left(\frac{a}{\eta}\right)^2\frac{\mathrm{d}\eta}{\mathrm{d}t} \qquad \text{(II 12)}$$

from equation (II 4). Hence

$$\frac{d\eta'}{dt'} = 2\left(\frac{\eta'}{a'}\right)\frac{da'}{dt'}, \tag{II 13}$$

where $\eta' = \eta/R$ is equal to unity when $t' = 0$. Equation (II 5) may now be integrated and the minimum film thickness h_0 found for various combinations of We, R and $\rho T/\mu^2$. For water drops colliding in air, typical properties of the system are given in table 5.

The minimum film thickness is shown as a function of drop radius and Weber number for water-in-air collisions in figure 20; also shown in the figure are the experimentally determined critical values of We which define regions of bounce or coalescence. Film rupture at film thickness of between 0.30 and 0.25 μm is in good agreement with observation, thus there is evidence that this model is satisfactory from both the qualitative and quantitative point of view. Therefore, the criterion for coalescence is given approximately by $R < \frac{1}{4}(3\,We + 1)$ mm.

The electrostatic force between colliding drops

(a) *Drop deformation before impact*

If colliding drops are charged or are immersed in an external electric field, the electric field between the drops increases as they approach and the rate of drop distortion due to electric stress may be calculated approximately using the method of Brazier-Smith (1971). Hence, for drops which are initially spherical and of radius, R,

$$d^2\gamma/dt'^2 = \pi^2\epsilon E_n^2 R/2T, \tag{II 14}$$

where γ is the ratio of major and minor axes of the distorted drop, ϵ is the permittivity of the surrounding medium, and E_n is the electric field at the pole of a drop. If the drop volume is conserved, $\gamma = (\alpha/R)^{\frac{3}{2}}$, where α is the length of the major axis. The rate of change of normalized drop surface velocity can therefore be calculated from equation (II 14) and this quantity can be expressed as a rate of change of local Weber number. The resulting expression is

$$d\,We/dh' = -4\epsilon E_n^2 R/(3\,We\,T), \tag{II 15}$$

where $h' = h/R$. Equation (II 15) may be integrated by using the field-intensification results of Davis (1964) to give, approximately,

$$We^2 = We_0^2 - 8\epsilon E_0^2 R\{3(h' - h_0') + \ln(h'/h_0')\}/3T,$$

where E_0 is the strength of the uniform applied electric field at large distances from the drops, and We_0 and h_0' are the initial values of Weber number and normalized drop separation respectively. For water drops of about 1 mm radius, and for an applied field of $10^4\,V\,m^{-1}$, the predicted change in We is only about 10^{-2} before the effect of viscous film flow becomes important. Consequently, deformation of the drops before impact will only be effective in varying the local Weber number for drops approaching with very low We values or for cases of high electrification.

(b) *The electrostatic force across the film*

The electrical force between flattened drop surfaces may be calculated by using methods suggested by Foote (1971). For parallel surfaces with charge density σ the force per unit area normal to the surfaces is $\sigma^2/2\epsilon$. The total force over a surface of radius a is about two orders of magnitude less than forces calculated from equation (II 6), when drop charges are sufficient to

cause coalescence; these charges are much smaller than those required to deform the drop surface substantially.

If the drops are situated in an external electric field, the shape of the two-drop system may be assumed to be that of the prolate spheroid, as shown in figure 21 with major and minor semiaxes α and β respectively. The coordinate, ξ_0, in a prolate ellipsoid coordinate system ξ, θ, ζ provides that

$$\xi_0 = \alpha(\alpha^2 - \beta^2)^{-\frac{1}{2}}.$$

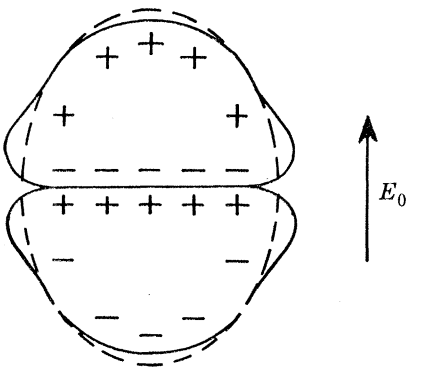

FIGURE 21. The approximation of the two-drop system by a spheroid.

Smythe (1950) gives the potential due to an external electric field E_0, parallel to the major axis, as

$$V = E_0(\alpha^2 - \beta^2)^{\frac{1}{2}}\xi\theta\{1 - (\operatorname{arcoth}\xi - \xi^{-1})/(\operatorname{arcoth}\xi_0 - \xi_0^{-1})\}.$$

The surface charge density may be calculated from

$$\sigma = -\epsilon\nabla V\cdot\boldsymbol{\eta},$$

where $\boldsymbol{\eta}$ is the unit surface normal. The charge on the exposed surface of each drop is found by integrating σ over θ. An equal and opposite charge of magnitude

$$Q = \pi(\alpha^2 - \beta^2)\,\epsilon E_0(\xi_0 \operatorname{arcoth}\xi_0 - 1)^{-1}$$

is therefore distributed over the parallel film surfaces. Since $\alpha \approx 2z_0$ and $\beta \approx R$, the factor $(\alpha^2 - \beta^2)(\xi_0 \operatorname{arcoth}\xi_0 - 1)^{-1}$ varies between $5.8R^2$ and $3R^2$ and therefore

$$Q \approx 4\pi\epsilon R^2 E_0.$$

Hence a field of $2.5 \times 10^3\,\mathrm{V\,m^{-1}}$ produces interface charge densities equivalent to those present if the drops carry equal and opposite charges of $4.4 \times 10^{-14}\,\mathrm{C}$ (cf. $6 \times 10^{-14}\,\mathrm{C}$ reported by Sartor & Abbott, 1968). The electrical forces produced by charges of this magnitude are too small to explain the observed enhanced coalescence.

INSTABILITY OF ELECTRIFIED FILM SURFACES

The stability of the film surfaces under the influence of electrical and surface forces may be studied by closely following the method used by Vrij (1966), who attempted to show how very thin films finally collapsed due to Van der Waals forces. Rectangular Cartesian coordinates x, y, z are used and the film is assumed to be square with sides of length $2a$. Since the film is essentially flat and much thinner than the diameter of the surfaces, discarding cylindrical symmetry in the theory of random surface fluctuations should cause negligible error.

The upper and lower surfaces are labelled 1 and 2 and have mean positions $z = \bar{h}$ and $z = 0$ respectively. The electrostatic potential energy per unit area, P, is

$$P = -\epsilon V^2/2h,$$

where V is the potential difference between the two interfaces and $h(x,y,t)$ is their separation. The combination of electrostatic and surface potential energies is

$$W = \iint_{\text{surfaces 1, 2}} T\,\mathrm{d}S = \iint_{\text{surfaces 1, 2}} P\,\mathrm{d}S,$$

where $\mathrm{d}S$ is an elemental area of the upper or lower surface given by

$$\mathrm{d}S = \{1 + (\partial z/\partial x)^2 + (\partial z/\partial y)^2\}^{\frac{1}{2}}\,\mathrm{d}x\,\mathrm{d}y$$

or for small fluctuations in film thickness,

$$\mathrm{d}S \approx \{1 + \tfrac{1}{2}(\partial z/\partial x)^2 + \tfrac{1}{2}(\partial z/\partial y)^2\}\,\mathrm{d}x\,\mathrm{d}y.$$

The electrostatic potential energy per unit area may be expanded in a Taylor series about its value for mean thickness $\bar{h}$:

$$P(h) \approx P(\bar{h}) + (\mathrm{d}P/\mathrm{d}h)_{\bar{h}}(h-\bar{h}) + \tfrac{1}{2}(\mathrm{d}^2P/\mathrm{d}h^2)_{\bar{h}}(h-\bar{h})^2.$$

The change in potential energy due to surface fluctuations is therefore

$$\Delta W \approx \iint \left[\tfrac{1}{2}T\left\{\left(\frac{\partial z_1}{\partial x}\right)^2 + \left(\frac{\partial z_1}{\partial y}\right)^2 + \left(\frac{\partial z_2}{\partial x}\right)^2 + \left(\frac{\partial z_2}{\partial y}\right)^2\right\} + \left(\frac{\mathrm{d}P}{\mathrm{d}h}\right)_{\bar{h}}(h-\bar{h}) + \frac{1}{2}\left(\frac{\mathrm{d}^2P}{\mathrm{d}h^2}\right)_{\bar{h}}(h-\bar{h})^2\right]\mathrm{d}x\,\mathrm{d}y.$$

The term in $\mathrm{d}P/\mathrm{d}h$ does not contribute to the integral since the mean of $h-\bar{h}$ is zero. Furthermore, the surface energy terms may be separated into components z_1+z_2, representing bending of the entire film, and components z_1-z_2, representing thickness fluctuations. The energy change for thickness fluctuations, ΔW, is therefore

$$\Delta W \approx \int\int_{-a}^{a} \left[\tfrac{1}{4}T\left\{\left(\frac{\partial h}{\partial x}\right)^2 + \left(\frac{\partial h}{\partial y}\right)^2\right\} + \frac{1}{2}\left(\frac{\mathrm{d}^2P}{\mathrm{d}h^2}\right)_{\bar{h}}(h-\bar{h})^2\right]\mathrm{d}x\,\mathrm{d}y.$$

The film thickness may be written as the sum of its Fourier components:

$$h = \bar{h} + \sum_{m=-\infty}^{+\infty}\sum_{n=-\infty}^{+\infty} H_{mn}\exp\{ik(mx+ny)\}, \tag{II 16}$$

where $k = \pi/a$ and $i = (-1)^{\frac{1}{2}}$. The combination of a wave m in the x direction with a wave n in the y direction results in an energy change

$$W_{mn} = 4a^2(H_{mn})^2\{\tfrac{1}{4}Tk^2(m^2+n^2) + \tfrac{1}{2}(\mathrm{d}^2P/\mathrm{d}h^2)_{\bar{h}}\}.$$

An m,n wave will therefore cause a decrease in potential energy if $(\mathrm{d}^2P/\mathrm{d}h^2)_{\bar{h}}$ is negative and if

$$\lambda > \lambda_C, \tag{II 17a}$$

where

$$\lambda = 2\pi/k(m^2+n^2)^{\frac{1}{2}} \tag{II 17b}$$

and

$$\lambda_C = \{-2\pi^2T/(\mathrm{d}^2P/\mathrm{d}h^2)_{\bar{h}}\}^{\frac{1}{2}}. \tag{II 17c}$$

Fluctuations with wavelength λ satisfying equation (II 17) will grow in amplitude and the film will be unstable. The further development of the instability is uncertain because the analysis

above has ignored the effects of the kinetic energy and viscous damping in the air film; however, this paper is only concerned with the onset of instability.

The Reynolds' equation now contains terms describing fluctuations as well as those describing mean film drainage. Because the equation is linear the two contributions may be separated and, in Cartesian coordinates,

$$\bar{h}^3\left(\frac{\partial^2\Delta p}{\partial x^2}+\frac{\partial^2\Delta p}{\partial y^2}\right)=12\mu\frac{\mathrm{d}h}{\mathrm{d}t}. \tag{II 18}$$

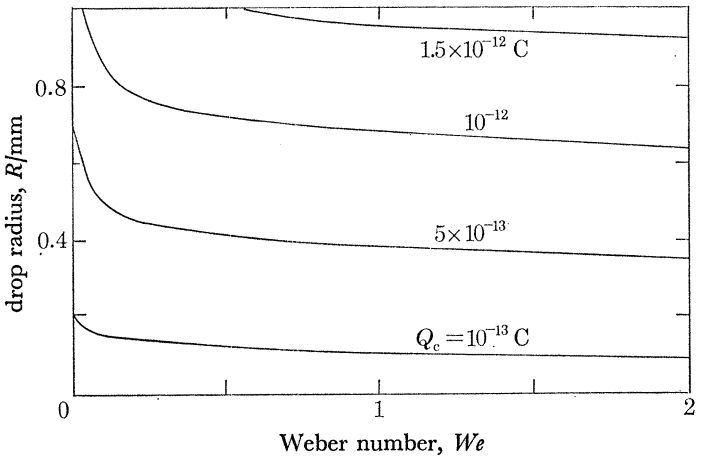

FIGURE 22. Critical drop charge for coalescence as a function of drop radius and Weber number.

The pressure change arising from fluctuations on both interfaces is given by

$$\Delta p = KT+2\Delta(\sigma^2/2\epsilon), \tag{II 19}$$

where K is the difference of surface curvatures

$$K \approx -(\partial^2 h/\partial x^2+\partial^2 h/\partial y^2). \tag{II 20}$$

Since $$\Delta(\sigma^2/2\epsilon)=\Delta\left(\frac{\mathrm{d}P}{\mathrm{d}h}\right)\approx\left\{\left(\frac{\mathrm{d}P}{\mathrm{d}h}\right)_{\bar{h}}+\left(\frac{\mathrm{d}^2P}{\mathrm{d}h^2}\right)_{\bar{h}}(h-\bar{h})\right\}-\left(\frac{\mathrm{d}P}{\mathrm{d}h}\right)_{\bar{h}}$$

substitution of equations (II 19) and (II 20) into equation (II 18) yields

$$\frac{\mathrm{d}h}{\mathrm{d}t}=(\bar{h}^3/12\mu)\left\{2\left(\frac{\mathrm{d}^2P}{\mathrm{d}h^2}\right)_{\bar{h}}\left(\frac{\partial^2 h}{\partial x^2}+\frac{\partial^2 h}{\partial y^2}\right)-T\left(\frac{\partial^4 h}{\partial x^4}+\frac{\partial^4 h}{\partial x^2\partial y^2}+\frac{\partial^4 h}{\partial y^4}\right)\right\}. \tag{II 21}$$

Substitution of equation (II 21) into equation (II 16) gives

$$\mathrm{d}H_{mn}/\mathrm{d}t=-H_{mn}(\bar{h}^3/12\mu)\,[2(\mathrm{d}^2P/\mathrm{d}h^2)_{\bar{h}}\,k^2(m^2+n^2)+Tk^4(m^2+n^2)^2]. \tag{II 22}$$

Hence $$H_{mn}(t)=H_{mn}(0)\exp(t/\tau),$$

where, from equations (II 22) and (II 17),

$$1/\tau=(4\pi^4T\bar{h}^3/3\mu\lambda^2)(\lambda_{\mathrm{C}}^{-2}-\lambda^{-2}).$$

If $\lambda>\lambda_{\mathrm{c}}$ then $\tau>0$ and a fluctuation of wavelength λ will increase exponentially with time. The most rapidly increasing fluctuation is that for which τ is a minimum, and $\lambda=\sqrt{2}\,\lambda_{\mathrm{c}}$. If

$2a > \lambda_c$, a fluctuation with $\lambda > \lambda_c$ always exists and the inequality can thus be used as an approximate stability condition. This condition may be written as

$$\bar{h}^3 \leqslant 2\epsilon a^2 V^2/\pi^2 T.$$

Hence

$$\bar{h} \leqslant 2\epsilon a^2 E_n^2/\pi^2 T \quad \text{or} \quad \bar{h} \leqslant Q^2/(2\pi^2 \epsilon a^2 T).$$

By using calculated minimum values of $\bar{h}$ and corresponding values of a, the minimum drop charge, Q_c required to initiate coalescence may be calculated and plotted as a function of R and We; this is shown in figure 22. The drop charges are much higher than those found experimentally but this is not surprising if one considers that the stability criterion is only an approximate one. The form of dependence of Q_c on both R and We, however, agrees with experiment. Since Q_c is almost independent of We, increasing drop charge above a critical value will cause drops of a particular size to always coalesce on impact, regardless of impact velocity. This prediction is in agreement with results of Gunn (1965*b*) and Sartor & Abbott (1968) who found that bouncing could always be suppressed by exceeding a certain critical drop charge or applied electric field.

Summary

The stability of the film trapped between colliding drops has been examined for both neutral and electrified cases. The stability of the film for neutral drops is found to be closely linked to drop deformation. A simple theory for drop flattening on impact allows drop deformation to be modelled and the minimum film thickness to be found. Predicted relations between minimum thickness, drop radius, and impact conditions agree quantitatively and qualitatively with experimentally determined ones. Various theories by other workers of enhanced film thinning due to electrical forces have been examined and have been found to be less successful. The theory described here, which is based on an examination of the stability of charged interfaces in the presence of surface waves, predicts critical drop charges to within an order of magnitude of those found experimentally.

III. A PARAMETRIC METHOD FOR THE INVESTIGATION OF THE STABILITY OF LARGE LIQUID DROPS

A method is described which permits the determination of the stability criteria for liquid drops. Any given physical situation may be parameterized into components which are independent of drop shape and other components which are dependent on drop shape; the latter components may be interrelated by providing certain shape constraints. A knowledge of the input parameters which are shape independent then provides solutions for the extremes of drop shape. In many cases, the treatment is essentially two-dimensional and is amenable to graphical methods of solution. Treatments are given of an isolated ellipsoidal drop situated in an intense electric field; a rotating, oscillating ellipsoidal drop; asymmetric breakup of pairs of unequal-sized drops after collision. The method investigates rotational, electrostatic, and surface energy contributions at moments in time when the kinetic energy of oscillation is a minimum. Attention is drawn to the erroneous assumption made by previous workers that stability criteria may be rigorously established by regarding the zero kinetic energy condition as an equilibrium one. It is further shown that for asymmetric collisions viscosity plays an important rôle in determining drop stability; previous investigators have assumed that viscosity effects can be neglected.

Introduction

Many workers, for example, Appell (1932), Sperber (1962), Chandrasekhar (1965), and Cohen *et al.* (1974), have considered the solution of dimensionless equations to determine the equilibrium shape of rotating fluid drops. In determining such solutions, a necessary condition is that the kinetic energy of the drop, measured in its centre-of-mass frame, is zero for all time. Brazier-Smith *et al.* (1971) have used the equilibrium solution to explain drop instability; it is emphasized here that such a procedure is incorrect.

An investigation of drop stability, however, may be undertaken by considering conditions when the kinetic energy is a minimum (for example, at the extreme limits of oscillation). The treatment described below examines drop motion in terms of two sets of dimensionless energy terms, one set defining the shape-independent components of electrostatic, rotational, and total energy of the system, and the other set defining the shape-dependent components of surface, electrostatic and rotational energy involved. A solution is effected by applying some physically realistic shape constraint to the system which leads to a unique relation between the shape-dependent parameters; the behaviour of the system is then determined by the shape-independent parameters.

It is shown below that solutions of drop shape and criteria for drop instability may be obtained in a convenient and illuminating manner by a graphical method of wide applicability.

The graphical technique

Equation (I 3) may be rewritten

$$\xi_K + A_S + 2e_C A_C + e_R A_R = e_T. \tag{III 1}$$

At certain times, t, $\partial \xi_K(t)/\partial t = 0$, though only instantaneously, and equation (III 1) reduces to

$$\partial (A_S + 2e_C A_C + e_R A_R)/\partial t = 0, \tag{III 2}$$

and definition of the parameters e_C, e_R and e_T leads to a relation between the unknown quantities A_S, A_C, and A_R. It remains to choose a shape constraint as a model for the liquid-drop system thereby leading to a further relation between A_S, A_C, and A_R which describes a surface in $A_S - A_C - A_R$ space. This surface is intersected by the plane represented by equation (III 2), the points of intersection therefore identifying solutions $[A_S, A_C, A_R](t)$. It is emphasized that the solutions are not equilibrium states but configurations of minimum kinetic energy. The analysis is considerably simplified if ξ_K is assumed to be much smaller than e_T whenever ξ_K is a minimum. This assumption is justified later by comparing predictions of the analysis with known results. Then equation (III 1) may be written

$$A_S + 2e_C A_C + e_R A_R = e_T. \tag{III 3}$$

It frequently occurs that one of the quantities e_C and e_R may be neglected or is zero so that the problem becomes two-dimensional. For example, the effect of electrostatic forces may be negligible so that equation (III 3) becomes

$$A_S + e_R A_R = e_T \tag{III 4}$$

and defines a straight line in the $A_S - A_R$ plane. If, for such a system, a shape-constraint function is found which relates A_R to A_S, then the two nonlinear equations may be solved for A_R, A_S and

hence drop shape. Because of the complexity of the relation between A_S and A_R a graphical analysis is useful. Figure 23 shows the general properties of the parametric shape-constraint curve and the energy line.

The intercepts of the straight line represented by equation (III 4) with the parametric shape-constraint curve then define the drop shape at the limits of deformation. If one of these limits does not exist for a particular combination of e_R and e_T then deformation is unlimited and the drop system is unstable. In addition, permissible drop shapes must lie to the left of the energy line since this is a necessary condition for kinetic energy to be positive. Energy lines with more than one intercept with the parametric shape restraint curve correspond to a physically stable system.

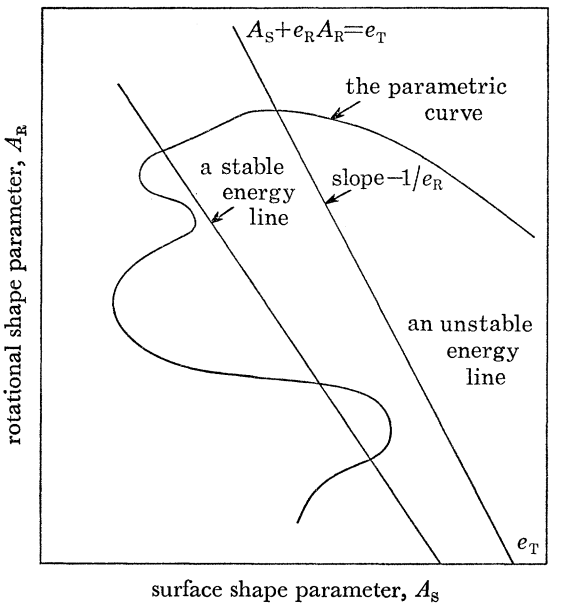

FIGURE 23. The parametric shape-constraint curve and energy line. Each point on the parametric curve defines a particular drop shapes. The unstable energy line has only one intercept with the parametric curve; the stable energy line has more than one. All drop shapes must lie to the left of the energy line; this is the condition that the kinetic energy is positive.

APPLICATIONS OF THE METHOD

(*a*) *Ellipsoidal drop immersed in a strong electric field*

An excellent example of the use of the parametric method is provided by the much-studied case of an isolated ellipsoid situated in an intense electric field. For most circumstances, the terms e_R and A_R may be neglected and interest conentrated upon the relation between the dimensionless quantities A_C, A_S, e_C and e_T. Thus equation (III 3) becomes

$$A_S + 2e_C A_C = e_T, \tag{III 5}$$

which is the energy line in the $A_S - A_C$ plane.

Drop shape is defined by a single parameter, the axial ratio, γ. It can be shown that

$$A_C = \gamma^2/3\Pi, \tag{III 6}$$

where

$$\Pi = (1/2e^3)\ln\{(1+e)/(1-e)\} - 1/e^2$$

and

$$e^2 = 1-\gamma^{-2}.$$

For oblate ellipsoids, $$A_S = \tfrac{1}{2}\gamma^{-\frac{2}{3}}\{1 + (\gamma^2/2\epsilon)\ln[(1+\epsilon)/(1-\epsilon)]\}, \quad \text{(III 7}a\text{)}$$

where $$\epsilon^2 = 1 - \gamma^2.$$

For prolate ellipsoids, $$A_S = \tfrac{1}{2}\gamma^{-\frac{2}{3}}\{1 + (\gamma/e)\arcsin e\}. \quad \text{(III 7}b\text{)}$$

The equations (III 6)–(III 7) relate A_C and A_S through the parameter γ, and constitute a parametric curve $A_C = A_C(\gamma)$; $A_S = A_S(\gamma)$ in the $A_C - A_S$ plane. This curve is shown in figure 24 together with two straight lines representing equation (III 5) for two sets of e_C and e_T. One line, A, indicates a case of stable drop oscillation, but the other line, B, only intersects the parametric curve once and examination shows the drop to be oblate at this point. This is not an equilibrium shape for the drop and so movement toward a prolate shape will ensue. However, no prolate shape is possible which will satisfy equation (III 5), and so the drop becomes unstable. A close examination of figure 24, using a considerably enlarged detail, showed excellent agreement with the results obtained analytically by Brazier-Smith (1971).

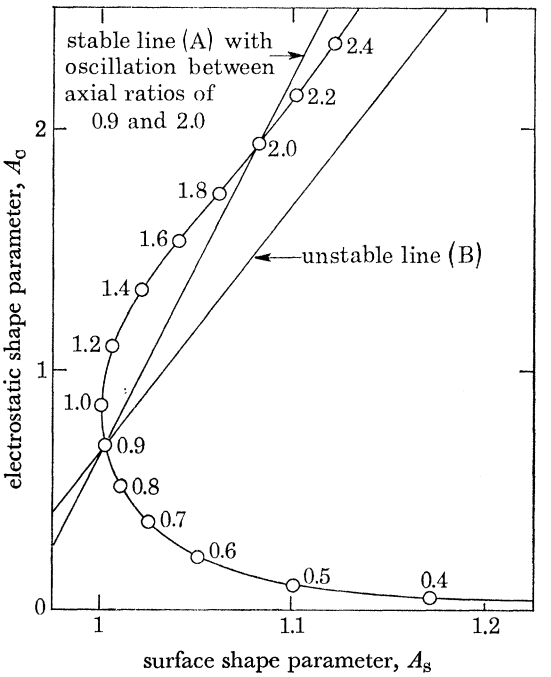

FIGURE 24. The ellipsoidal parametric shape-constraint curve for an oscillating drop situated in a strong external electric field. Values of the axial ratio parameter are indicated along the curve.

It is possible for the energy line to contact the parametric restraint curve tangentially, so that the two intercepts coincide and indicate a true equilibrium shape of a spheroid in an electric field. Such tangential lines (for $1.4 < \gamma < 1.8$) also have a third intercept at high values of A_C; this agrees with the usual analysis which predicts two values of γ for a particular external field. As the slope of the tangent line increases, all three intercepts become closer and may coincide, When this occurs, at the flat portion of the parametric curve, where $\gamma = 1.8$, the ellipsoid is in unstable equilibrium, in close agreement with conventional theory.

In figure 24, vertical energy lines represent free drop oscillation in the absence of an electric field and thus the axial ratios corresponding to oscillation limits can be read directly from the figure. The tangential coincident intercept, in the absence of an electric field, occurs at $\gamma = 1$

when the shape is a sphere; this is the equilibrium shape. Limiting axial ratios agree with the classical theory (see Lamb 1932, for example).

(*b*) *The rotating, oscillating ellipsoid*

After the impact of two freely falling drops, the agglomerate mass may be conveniently approximated by an ellipsoidal shape, so that

$$A_{\mathrm{R}} = 2\gamma^{\frac{2}{3}}/(1+\gamma^2).$$

The corresponding parametric curve is shown in figure 25, with energy lines taking the form of equation (III 4), and is totally different in form from the previous case. Although tangential intercepts representing equilibrium rotation are possible, in no instance is drop instability predicted. Classical investigations of rotating ellipsoids (Maclaurin spheroids, Jacobi ellipsoids, Poincaré pears, etc.) have not been restricted to rotational symmetry and as such give slightly more accurate estimates of equilibrium drop shape (see Lamb 1932). Instability in these instances is due to deformation into non-ellipsoidal shapes.

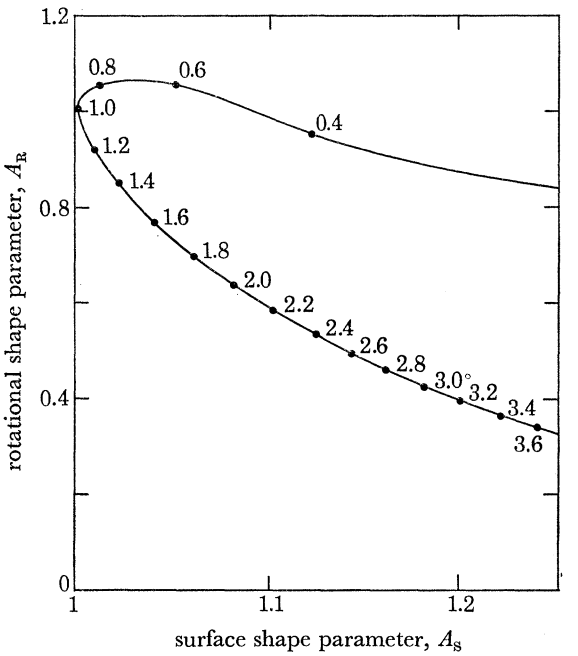

FIGURE 25. The parametric shape-constraint curve for a rotating oscillating ellipsoidal drop. Values of the axial ratio parameter are indicated along the curve.

The unconditional stability of a drop which is confined to an ellipsoidal shape is not surprising. With increasing axial ratio, the rotational energy decreases but surface energy can increase without bound. Since there is no maximum for the surface energy, a point of instability is never reached. As discussed by Brazier-Smith (1971), however, the spheroidal assumption is limited because of coupling with other oscillation modes during finite oscillations. The largest natural oscillations recorded appear to be $\gamma_{\max} - \gamma_{\min} = 0.9$ reported by Jones (1959), and this suggests that the validity of a spheroidal stability analysis would be restricted to the top left-hand peak of the parametric shape constraint curve.

There are other deficiencies of the ellipsoidal model. It is unrealistic for collisions between drops of unequal size, and it does not predict the waist which is observed during oscillation. Furthermore, collisions between drops of equal size are very rare occurrences in nature.

(*c*) *Non-symmetrical rotating liquid masses*

If it is required to investigate the collision of drops of unequal size, a suitable shape–constraint model must be found to describe the agglomerate mass bearing in mind that the degree of non-symmetry should correspond to the difference in radius of the incident drops. A model is proposed here which is based upon the theory for locating equipotential surfaces in the vicinity of an array of point charges. Justification for the model is that if potential flow conditions are assumed within the liquid mass, the surfaces described in both the electrostatic system and the fluid system are those which satisfy the equation of Laplace; also in both systems the mechanical forces exerted are perpendicular to the equipotential surfaces. Inspection of the equipotential surfaces generated by unequal point charges shows a marked similarity to photographs of the drop shape following the collision and during breakup of drops of unequal size.

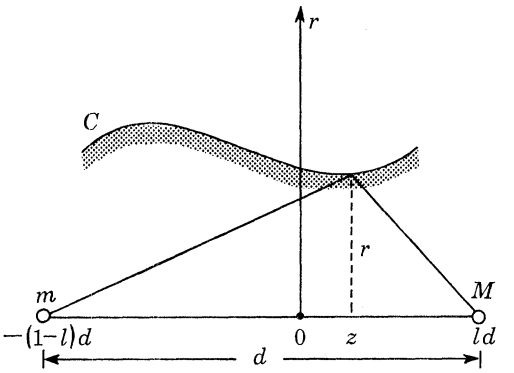

FIGURE 26. The geometry used to determine equipotential surfaces surrounding liquid drops of mass M and m separated by a distance d.

A suitable mapping is therefore obtained for liquid drops of mass M and m by taking an origin at the centre of mass and drawing equipotentials corresponding to charges of value M and m. From figure 26, and writing $l = m/(M+m)$,

$$C = l[r^2+\{z+(1-l)\,d\}^2]^{-\frac{1}{2}} + (1-l)[r^2+\{z-ld\}^2]^{-\frac{1}{2}}, \qquad \text{(III 8)}$$

where C is a constant (equipotential). Such an equation, in which r and z are present to the eighth power is cumbersome. However, computation showed that the fourth degree equation

$$C = l[r^2+\{z+(1-l)\,d\}^2]^{-1} + (1-l)[r^2+\{z-ld\}^2]^{-1} \qquad \text{(III 9)}$$

describes almost identical 'equipotential' surfaces which have similar properties to those of equation (III 8). Figure 27 shows two examples which use equation (III 9) of the deformation of a sphere which result in breakup. Curves (*a*) of figure 27 demonstrate symmetrical deformation ($l = 0.5$), and curves (*b*) demonstrate asymmetrical deformation, where $l = 0.05$. In each case the mass ratio of the drops at breakup, m/M, was that appropriate to the value of l used in equation (III 8), but the elongation before breakup is less than that determined from the investigation described in part I. An increase in elongation may be achieved in the mapping model by

using a multipole expansion of the drop surface, say by using two pairs of colinear masses, but no such attempt has been made in the present work. Satellite drop production caused by Rayleigh jet rupture may be modelled by a multipole expansion representing a line of lesser masses placed between the major masses; the effect of the lesser masses only becomes evident as a filament develops.

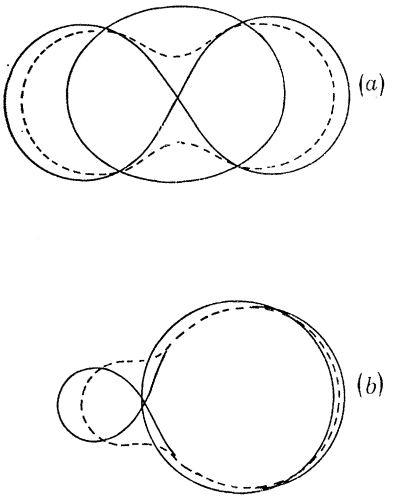

FIGURE 27. Stages in the development of symmetrical and asymmetrical breakup according to the equipotential model.

The parametric shape constraint curve is shown for several values of l in figure 28 and may be used to investigate the drop behaviour resulting from a collision between pairs of drops of unequal size. Equal masses ($l = 0.5$) have a similar form of curve to the ellipsoidal parametric curve previously discussed, except for the breakup shown in figure 28 to occur at $A_S \approx 1.28$. Breakup is due to the separation of the fragments when the diameter of the neck becomes zero. The curves for other values of l progressively depart from the ellipsoidal form. Only that part of the curve for which the drop is prolate in character is known; it is assumed that a curve similar to the ellipsoidal case describes shapes which are oblate in character. It is the prolate portion of the parametric curve which determines the point of instability. Two limiting cases of stability arise and are discussed below.

(*d*) *Criteria for stability following a collision*

(i) *Critical impact parameter*

In a two-drop system it is possible to maintain the kinetic energy at a constant value while independently varying the energy of rotation. This is equivalent to considering impacts where the relative velocity is fixed but the separation of drop trajectories in the centre of mass frame is allowed to vary. Then, if the relative velocity is sufficiently large, a critical impact parameter (or separation) will exist such that the increased rotational energy will result in instability and breakup. This is the condition which has been erroneously treated by Brazier-Smith *et al.* (1971) as an equilibrium state.

From equation (III 1) the initial energy condition is

$$A_S^{(i)} + e_R A_R^{(i)} = e_T - \xi_K^{(i)}, \qquad \text{(III 10)}$$

where the superscript (i) refers to the values of the initial energy states. The energy line in this case, for which $\xi_K(t) = 0$, is given by equation (III 4), and it follows that the point $(A_S^{(i)} + \xi_K^{(i)}, A_R^{(i)})$ in the $A_S - A_R$ plane will lie on this line for all values of e_R. Since the initial kinetic energy $\xi_K^{(i)}$ is held constant, the point $(A_S^{(i)} + \xi_K^{(i)}, A_R^{(i)})$ becomes a pivotal point for all energy lines describing the condition $\xi_K(t) = 0$. From figure 29*a* it may be deduced that the slope of such energy lines must exceed a certain limit if the line is to pass through the pivotal point and also intersect the parametric curve. This limit is expressed by the condition

$$\frac{e_T - (A_S^{(i)} + \xi_K^{(i)})}{A_R^{(i)}} \leqslant \frac{A_S^{(b)} - (A_S^{(i)} + \xi_K^{(i)})}{A_R^{(i)} - A_R^{(b)}}, \qquad \text{(III 11)}$$

where the superscript (b) refers to the values of the energy states at the moment of breakup.

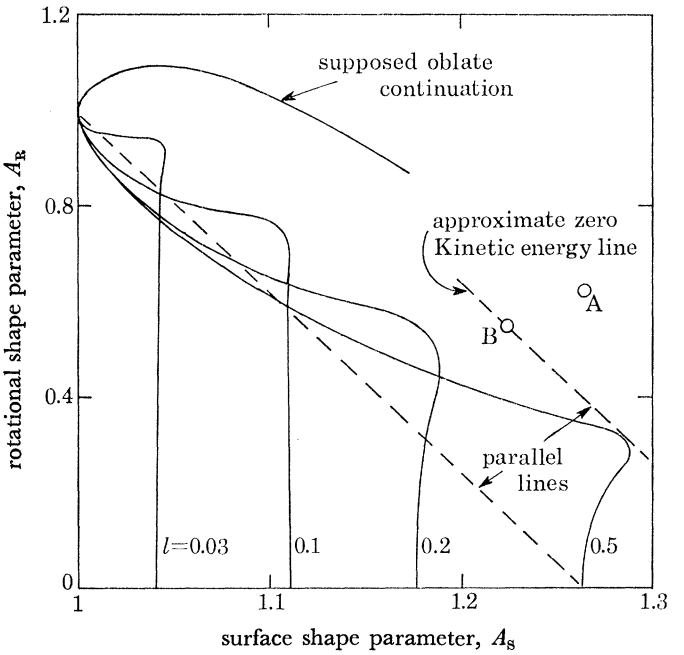

FIGURE 28. A set of parametric shape-constraint curves for collisions between drops of unequal radii. Breakup occurs at the knee of each curve. Points A and B are discussed in the text.

Equation (III 11) overestimates the limiting slope for stability because the energy loss due to viscous dissipation is not accounted for. The energy dissipation during drop oscillation following a collision may be developed for small oscillations from the theory given by Lamb (1932); calculations performed by Foote (1973) for the case of finite oscillations agree closely with this theory. The viscous energy loss is proportional to the sum of kinetic energy and potential energy, and can be written as $n(e_T - 1)$ where n depends upon the number of oscillations performed by the drop. The corresponding energy line at breakup, for which $\xi_K(t) = 0$, is therefore

$$\begin{aligned} A_S + e_R A_R &= e_T - n(e_T - 1) \\ &= (1 - n)\, e_T + n. \end{aligned} \qquad \text{(III 12)}$$

From equation (III 10), the point $(\{A_S^{(i)}+\xi_K^{(i)}\}\{1-n\}+n,\ A_R^{(i)}\{1-n\})$ therefore lies on the line defined by equation (III 14) and is the new pivotal point shown in figure 29*b*. Thus the stability condition of equation (III 11) is replaced by

$$\frac{e_T(1-n)+n-\{(A_S^{(i)}+\xi_K^{(i)})(1-n)+n\}}{A_R^{(i)}(1-n)} \leqslant \frac{A_S^{(b)}-\{(A_S^{(i)}+\xi_K^{(i)})(1-n)+n\}}{A_R^{(i)}(1-n)-A_R^{(b)}},$$

which may be rearranged to give

$$e_R \leqslant \frac{A_S^{(b)}-(A_S^{(i)}+\xi_K^{(i)})(1-n)-n}{A_R^{(i)}(1-n)-A_R^{(b)}}. \qquad \text{(III 13)}$$

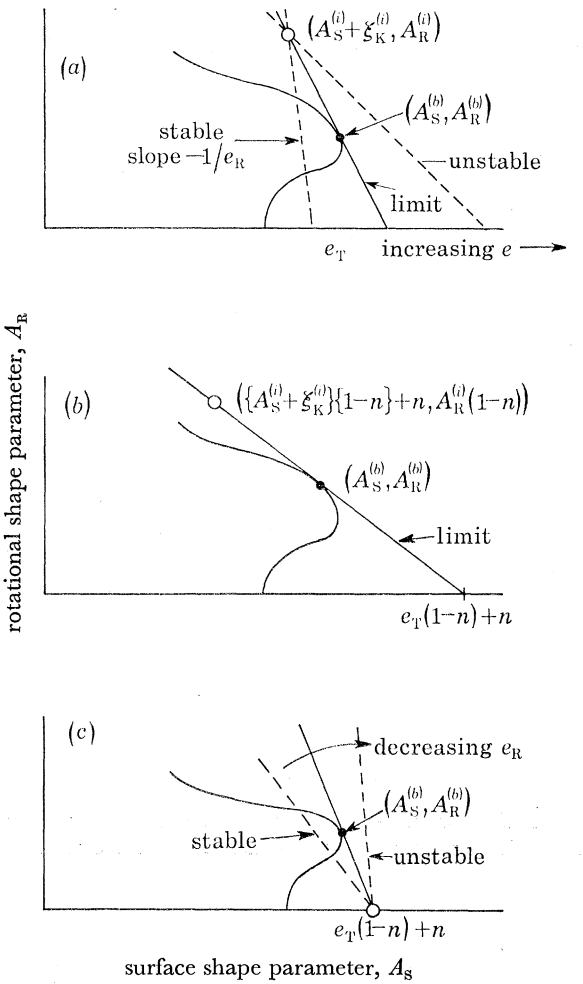

FIGURE 29. (*a*) the determination of the upper limit of e_R for drop stability; (*b*) the determination of the upper limit of e_R when the effect of viscous dissipation is included; (*c*) the determination of the lower limit of e_R for drop stability, assuming that the total energy, e_T, is held constant.

For a single cycle of ellipsoidal-mode oscillation, theory by Lamb (1932) predicts that

$$n = 1-\exp\{-10\nu\pi(\rho/2TR)^{\frac{1}{2}}\},$$

where ν is the kinematic viscosity, ρ is the density, T is the surface tension of water, and R is the drop radius. The value of n increases as R increases and, for example, $n = 0.14$ when $R = 0.6$ mm. The initial point $(A_S^{(i)}+\xi_K^{(i)},\ A_R^{(i)})$ and the corrected pivotal point $(0.86\,A_S^{(i)}+\xi_K^{(i)}+0.14,\ 0.86\,A_R^{(i)})$

are shown in figure 28 as the points A and B respectively. The limiting line for stability drawn through point B is very nearly parallel to the line through (1, 1) and $(A_S^{(i)}, 0)$, which is also indicated in figure 28. This suggests that equation (III 13) could be re-expressed in terms of the gradient of this parallel line by

$$e_R \leqslant (A_S^{(i)} - 1)/(1 - 0) = A_S^{(i)} - 1. \qquad \text{(III 14)}$$

Equation (III 14) is the condition of stability obtained by Brazier-Smith *et al.* (1971) by entirely different reasoning and, although the assumptions they made in obtaining this solution were not stated explicitly, it is important to investigate these carefully. They assumed that the colliding drops formed a sphere having zero kinetic energy and that the limiting case was associated with a disintegration which produced two spheres having the same radii as the initial colliding drops. The separating drops were assumed by Brazier-Smith *et al.* (1971) to have zero kinetic energy and zero rotational energy. The case in which colliding drops attain a spherical shape having zero kinetic energy is a very special case indeed; for almost all time, the agglomerated mass resulting from a collision may be expected to suffer severe distortion. In view of the particular assumptions made by Brazier-Smith *et al.* (1971), the agreement between their criterion for stability and their experimental data appears to be fortuitous.

The approximate criterion for instability, given by equation (III 14) is expected to be valid for the collisions between drops of different radius provided that the radius ratio of the incident drops does not exceed 3; where the ratio exceeds this value, the slope of the limiting energy line will exceed $(A_S^{(i)} - 1)^{-1}$. A more quantitative evaluation is not possible without data on the viscous energy loss in asymmetric collisions. It remains, however, that viscosity is of appreciable importance in determining stability; previous investigators have assumed that viscosity was a factor which could be ignored in such calculations.

(ii) *Critical total energy parameter*

The second criterion of stability is that the total energy, e_T, must not exceed the minimum to cause drop breakup. This condition may be written

$$e_T - n(e_T - 1) \leqslant e_R A_R^{(b)} + A_S^{(b)}$$

so that stability is achieved when

$$\{(1-n)e_T + n - A_S^{(b)}\}/A_R^{(b)} \leqslant e_R \leqslant A_S^{(i)} - 1, \qquad \text{(III 15)}$$

the first inequality being illustrated in figure 29*c*. Two bounds are thus imposed upon the parameter e_R which are investigated further.

(iii) *A test of the stability criteria*

Consider a drop of radius R impacting with a smaller drop of radius r at a speed relative to the latter of U.

The values of $A_R^{(b)}$ and $A_S^{(b)}$ may be related to the initial values of $A_R^{(i)}$ and $A_S^{(i)}$ through the expressions

$$A_R^{(b)} = \Psi_R A_R^{(i)}, \quad A_S^{(b)} = \Psi_S A_S^{(i)},$$

where Ψ_R and Ψ_S are unknown functions, and substituting for e_R and e_T from part I, equation (III 15) becomes

$$(1+\beta^3)\Psi_R[1-n+6\{(1-n-\Psi_S)(1+\beta^2)+n(1+\beta^3)^{\frac{2}{3}}\}(1+\beta^3)/(\beta^3 We)] < X^2 < 12[\{1+\beta^2-(1+\beta^3)^{\frac{2}{3}}\}(1+\beta^3)^{\frac{1}{3}}][5\beta^6(1+\beta)^2 We], \qquad \text{(III 16)}$$

where $\beta = R/r$, and We is the Weber number $= r\rho U^2/\sigma$.

The form of equation (III 16) is

$$1 - b/U^2 < X^2 < c/U^2,$$

where a, b, and c are constants dependent upon the values of the radius of the incident drops. The function defined by equation (III 16) is compared with the experimental results of Adam *et al.* (1968). Values of Ψ_S and Ψ_R are taken from figure 28 and the results of the comparison are shown in figure 30. The theory given here is seen to predict accurately the upper limit for X, but the lower limit is not well estimated. The poor fit to the lower limit of X is not unexpected, since the nature of the instability modelled here assumes that breakup will occur when the aggregate drop reaches an extreme prolate shape. In fact, the experiments described in part I demonstrate an onset of instability at a moment when an extreme oblate shape occurs. When the drop assumes a disk-like shape, waves form around the perimeter of the disk and become rapidly amplified until the disk folds along a diameter. A prolate shape is then rapidly formed and breakup follows: this form of instability is clearly much more complicated than that investigated above.

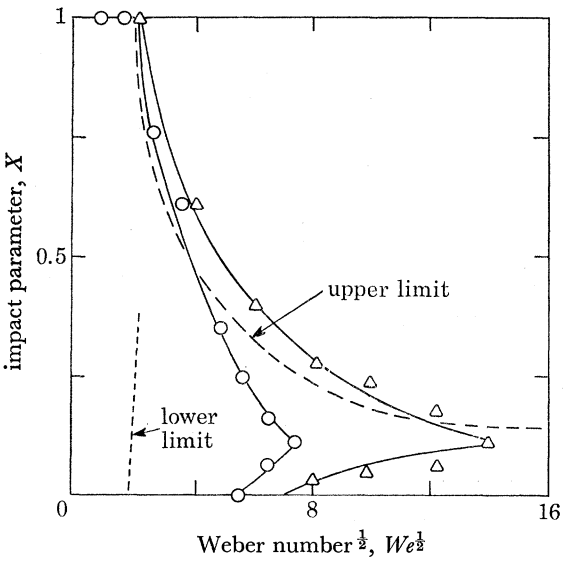

FIGURE 30. A comparison of the theoretical predictions of the limits of the impact parameter, X, as a function of the Weber number, We, to provide stable coalescence, with the experimental values of the limits as determined from the work of Adam *et al.* (1968) who studied the collisions of drops of equal size. ○, Drops of 60 μm radius; △, drops of 300 μm radius; – – –, theoretical prediction.

SUMMARY

A technique of wide applicability has been developed which allows drop stability to be investigated under very general conditions. A useful example is given of the technique applied to the oscillations of a spheroidal drop situated in an electric field. The coalescence problem proved far more difficult to treat, but some useful results on stability have emerged. A new method for the modelling of non-symmetrical breakup has been presented and extensions of the method discussed which could lead to interesting future work.

References

Adam, J. R., Lindblad, N. R. & Hendricks, C. D. 1968 *J. appl. Phys.* **39**, 5173–5180.
Appell, P. 1932 *Trâité de mecanique rationelle*. Paris: Gauthier-Villars.
Bradley, S. G. 1975 Ph.D. Dissertation, University of Auckland, Auckland, New Zealand.
Brazier-Smith, P. R. 1971 *J. Fluid Mech.* **50**, 417–430.
Brazier-Smith, P. R., Jennings, S. G. & Latham, J. 1971 *Proc. R. Soc. Lond.* A **326**, 393–408.
Cataneo, R. 1970 Unpublished manuscript quoted by Spengler & Gokhale (1973).
Chandrasekhar, S. 1965 *Proc. R. Soc. Lond.* A **286**, 1–26.
Charles, G. E. & Mason, S. G. 1960 *J. Colloid. Sci.* **15**, 236–267.
Cohen, S., Plasil, F. & Swiatecki, W. J. 1974 *Annls Phys.* **82**, 557–596.
Davis, M. H. 1964 *Q. J. Mech. appl. Math.* **17**, 499–511.
Foote, G. B. 1971 Ph.D. dissertation, University of Tucson, Tucson, Arizona.
Foote, G. B. 1973 *J. Comp. Phys.* **11**, 507–530.
Foote, G. B. 1975 *J. atmos. Sci.* **32**, 390–402.
Gillespie, T. & Rideal, E. K. 1956 *Trans. Faraday Soc.*, pp. 173–183.
Gunn, R. 1965*a* *Science, N.Y.* **150**, 695–701.
Gunn, R. 1965*b* *Science, N.Y.* **150**, 888–889.
Hartland, S. 1967 *Trans. Instn chem. Engrs* **45**, 102–108.
Hodgson, T. D. & Lee, J. C. 1969 *J. Colloid Sci.* **30**, 94–108.
Jayaratne, O. W. & Mason, B. J. 1964 *Proc. R. Soc. Lond.* A **280**, 545–565.
Jennings, S. G. & Latham, J. 1971 *Static Elec.* **10**, 84–92.
Jones, D. M. A. 1959 *J. Meteorol.* **15**, 504–510.
Lamb, H. 1932 *Hydrodynamics* (6th edition). New York: Dover Press.
List, R., MacNeil, C. F. & McTaggart-Cowan, J. D. 1970 *J. Geophys. Res.* **75**, 7573–7580.
MacKay, G. D. M. & Mason, S. G. 1963 *Can. J. chem. Engng* **41**, 203–212.
McTaggart-Cowan, J. D. & List, R. 1975 *J. atmos. Sci.* **32**, 1401–1411.
Magarvey, R. H. & Geldart, J. W. 1962 *J. atmos. Sci.* **19**, 107–113.
Mason, B. J. 1971 *The physics of clouds*, 2nd edition. Oxford: Clarendon Press.
Montgomery, D. N. 1971 *J. atmos. Sci.* **28**, 291–293.
Murdoch, P. G. & Leng, D. E. 1971 *Chem. Engng. Sci.* **26**, 1881–1892.
Nelson, A. R. & Gokhale, N. R. 1973 *J. Geophys. Res.* **78**, 1472–1474.
Owe Berg, T. G., Fernish, G. C. & Gaukler, T. A. 1963 *J. atmos. Sci.* **20**, 153–158.
Rayleigh, Lord. 1882 *Phil. Mag.* **14**, 184–186.
Reynolds, O. 1886 *Phil. Trans. R. Soc. Lond.* A **177**, 157–234.
Sartor, J. D. & Abbott, C. E. 1968 *J. Geophys. Res.* **73**, 6415–6423.
Sartor, J. D. & Abbott, C. E. 1972 *J. deRech. Atmos.* **6**, 479–493.
Schotland, R. M. 1960 *Discuss. Faraday Soc.* **30**, 72–77.
Sherman, F. S. 1958 *Proc. Second Biennial Gas Symp.*, pp. 134–142. Evanston: North-Western University Press.
Smythe, W. R. 1950 *Static and dynamic electricity* (2nd edition). New York: McGraw-Hill.
Spengler, J. D. & Gokhale, N. R. 1973 *J. Geophys. Res.* **78**, 497–503.
Sperber, D. 1962 *Phys. Rev.* **13**, 468–477.
Vrij, A. 1966 *Discuss. Faraday Soc.* **42**, 23–33.

PHILOSOPHICAL TRANSACTIONS OF THE ROYAL SOCIETY A MATHEMATICAL, PHYSICAL & ENGINEERING SCIENCES

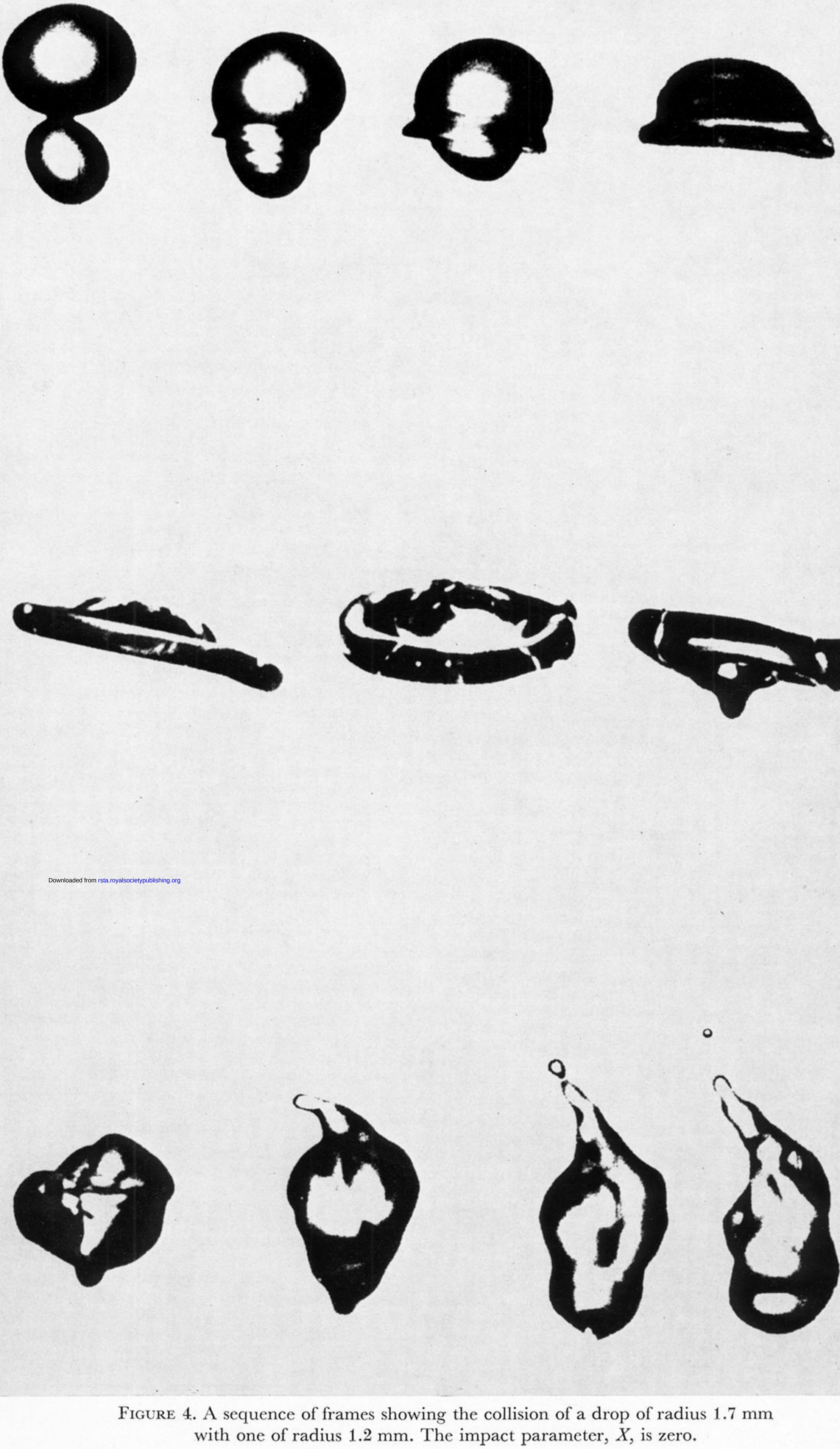

FIGURE 4. A sequence of frames showing the collision of a drop of radius 1.7 mm with one of radius 1.2 mm. The impact parameter, X, is zero.

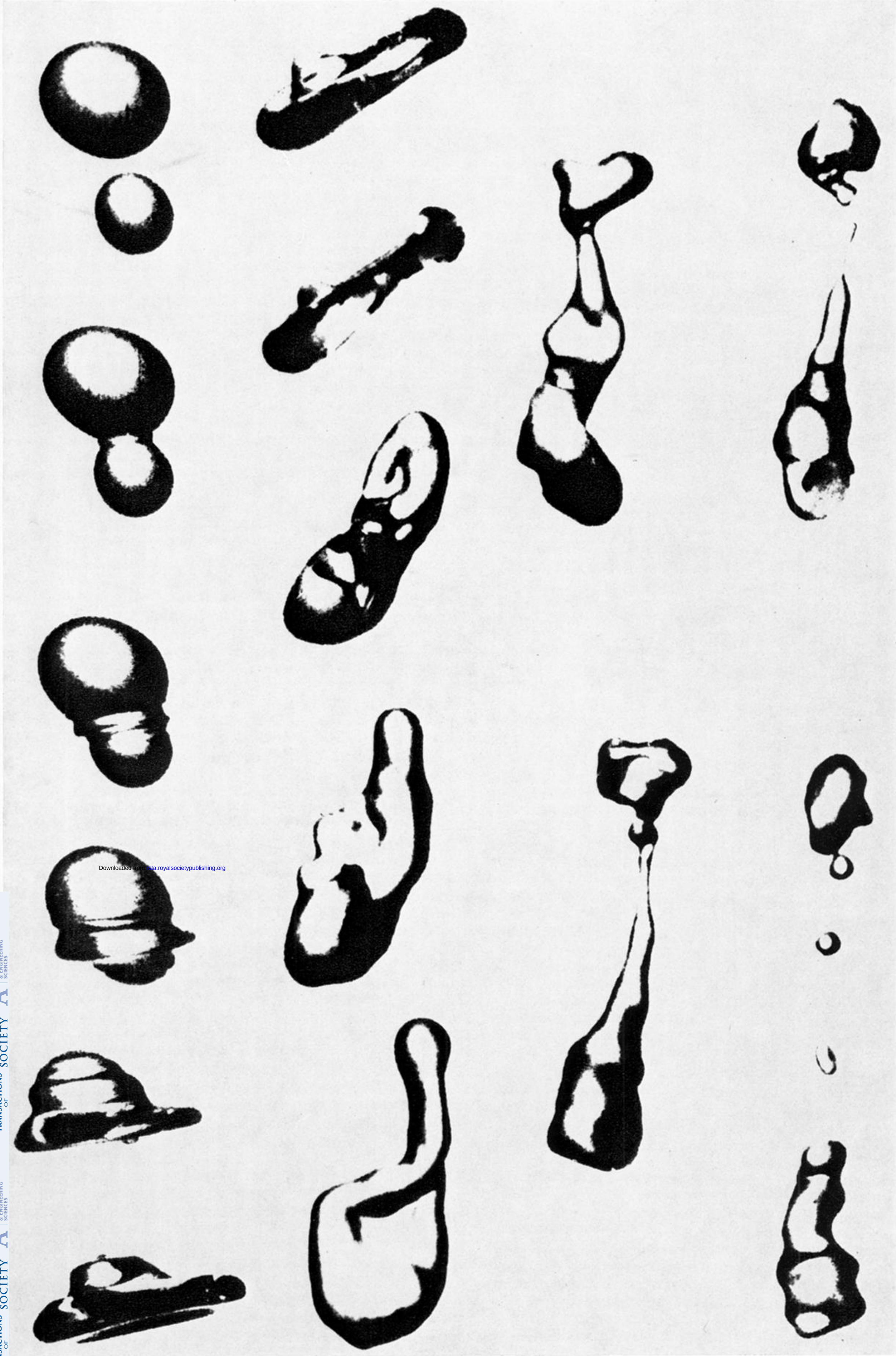

FIGURE 5. As for figure 4 but with the impact parameter, X, set to 0.35.
The series exemplifies disruption by rotation.

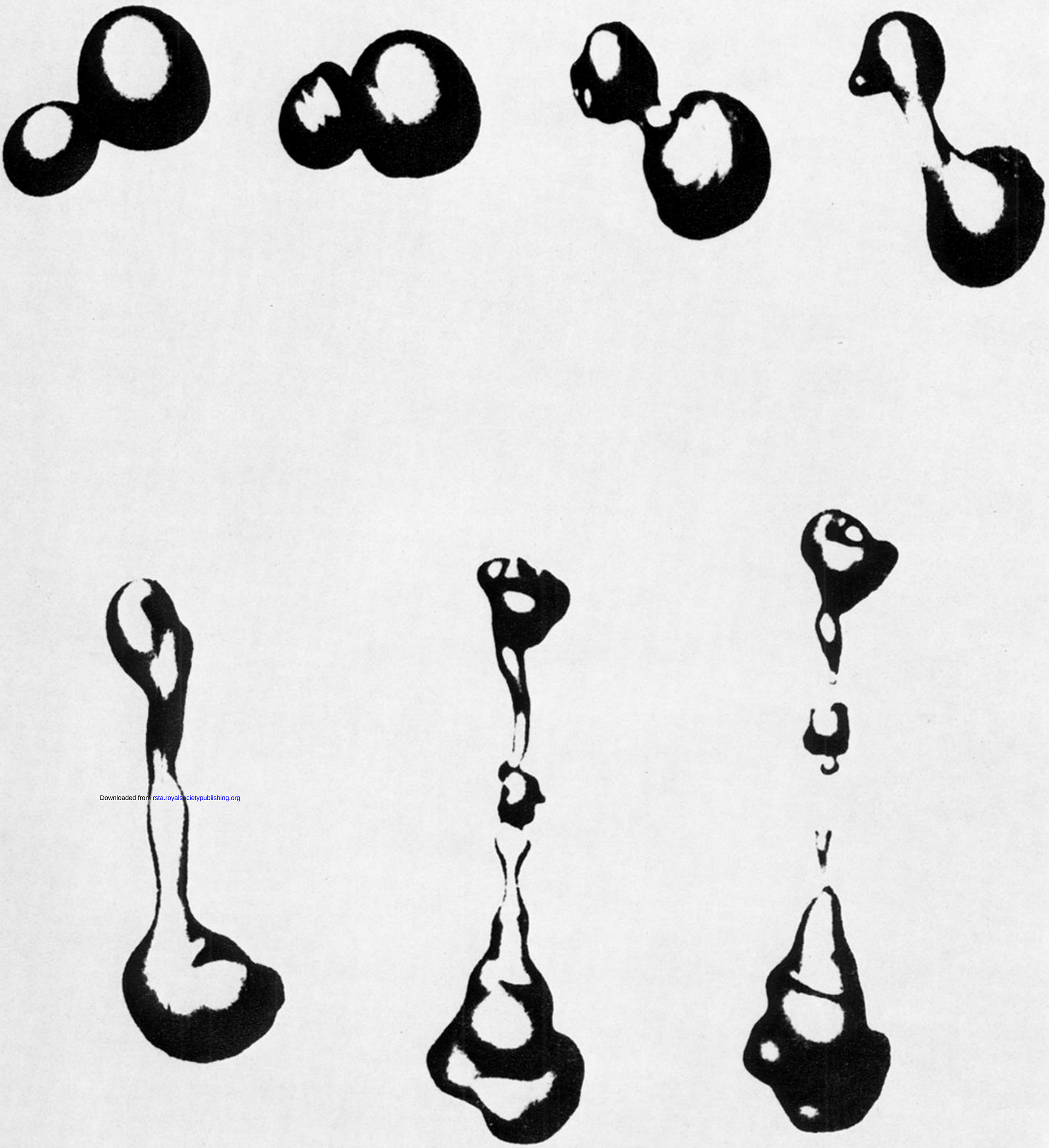

FIGURE 6. As for figure 4 but with the impact parameter, X, set to 0.90. The series shows disruption by a shearing action.